

# Stochastic sampling effects favor manual over digital contact tracing

Marco Mancastrrippa,<sup>1,2</sup> Claudio Castellano,<sup>3</sup> Alessandro Vezzani,<sup>4,1</sup> and Raffaella Burioni<sup>1,2</sup>

<sup>1</sup>*Dipartimento di Scienze Matematiche, Fisiche e Informatiche,  
Università degli Studi di Parma, Parco Area delle Scienze, 7/A 43124 Parma, Italy*

<sup>2</sup>*INFN, Sezione di Milano Bicocca, Gruppo Collegato di Parma,  
Parco Area delle Scienze, 7/A 43124 Parma, Italy*

<sup>3</sup>*Istituto dei Sistemi Complessi (ISC-CNR), Via dei Taurini 19, I-00185 Roma, Italy*

<sup>4</sup>*Istituto dei Materiali per l'Elettronica ed il Magnetismo (IMEM-CNR),  
Parco Area delle Scienze, 37/A-43124 Parma, Italy*

Isolation of symptomatic individuals, tracing and testing of their nonsymptomatic contacts are fundamental strategies for mitigating the current COVID-19 pandemic. The breaking of contagion chains relies on two complementary strategies: manual reconstruction of contacts based on interviews and a digital (app-based) privacy-preserving contact tracing. We compare their effectiveness using model parameters tailored to describe SARS-CoV-2 diffusion within the activity-driven model, a general empirically validated framework for network dynamics. We show that, even for equal probability of tracing a contact, manual tracing robustly performs better than the digital protocol, also taking into account the intrinsic delay and limited scalability of the manual procedure. This result is explained in terms of the stochastic sampling occurring during the case-by-case manual reconstruction of contacts, contrasted with the intrinsically prearranged nature of digital tracing, determined by the decision to adopt the app or not by each individual. The better performance of manual tracing is enhanced by heterogeneity in agent behavior: superspreaders not adopting the app are completely invisible to digital contact tracing, while they can be easily traced manually, due to their multiple contacts. We show that this intrinsic difference makes the manual procedure dominant in realistic hybrid protocols.

## I. INTRODUCTION

The current COVID-19 pandemic is impacting daily life worldwide at an unprecedented scale. Among the features that have contributed to transform the emerging diffusion of SARS-CoV-2 coronavirus into such a global scale crisis, a prominent role is played by the high rates of virus transmission mediated by presymptomatic and asymptomatic individuals [1–6]. Given the absence of effective pharmaceutical interventions, this feature makes the mitigation of the pandemic a highly nontrivial task, that has been tackled with various strategies, none of them devoid of drawbacks.

Initially, governments resorted to very restrictive limitations of non strictly necessary activities (lock-downs) to curb the diffusion of the infection. Such measures turned out to be effective from an epidemiological point of view, but exceedingly costly in other respects, for their economic and social consequences [7, 8]. Recently, such restrictive measures have been progressively lifted, and we now rely on other tools to contain the pandemic: social distancing, reinforced hygiene and the use of individual protection devices. Along with these provisions, aimed at preventing single virus transmission events, another set of measures points at breaking contagion chains: the isolation of infected individuals (symptomatic or found via some testing), followed by the tracing of their contacts (contact tracing, CT), the testing of the latter and the possible isolation of the infected [9–12].

This CT procedure has proven effective in the past in various contexts [13–16] but it comes, in its standard manual implementation, with important limitations [17].

It requires the set up of a physical infrastructure, needed to find infected individuals, interview them and reconstruct their contacts in a temporal window, call these contacts, convince them to get tested and eventually isolated. Apart from the evident problems of practical feasibility and economic cost, the manual CT procedure intrinsically implies a delay between the moment an individual is found infected (and isolated) and the time her contacts are tested and possibly isolated. For an epidemic such as COVID-19, characterized by a rather long presymptomatic infectious stage and a high relevance of transmission by asymptomatics, the delay implied by manual CT risks to undermine the effectiveness of the whole procedure.

For this reason the additional strategy of a digital CT procedure, based in particular on the installation of apps on smartphones (app-based), has been proposed alongside manual CT [2]. The rationale is that proximity sensors installed on these ubiquitous devices allow the detection of contacts of epidemiological significance among individuals. When an individual is found infected, the app permits to instantaneously trace all contacts in the recent past, thus allowing for much quicker testing and isolation. A quantitative comparison between manual and digital CT applied to an epidemiological model describing COVID-19 diffusion suggested that already a delay of the order of 3 days completely spoils the ability of manual CT to prevent the initial exponential growth of the epidemic [2]. The conclusion was that only a digital CT avoiding this delay could be a viable strategy to control the current epidemic. The proposal for digital CT rapidly gained momentum, leading to the development

of technical solutions [18–20] and to the deployment of app-based CT infrastructures in many countries [21].

Many works have scrutinized the actual validity of this solution and investigated the possible shortcomings of app-based CT, casting doubts over many of the assumptions underlying such strategy [22–24]: there are too few modern enough smartphones; Bluetooth based proximity measurements are unreliable; co-location is not always a good proxy for epidemiological contact. The potential risks for privacy breaches have also been exposed.

Other papers have tried to evaluate the impact of digital CT on the current COVID-19 epidemic, attempting to precisely determine, by means of detailed data-driven epidemiological models, to what extent such a strategy is able to suppress virus diffusion [25–29]. A critical role is played by the fraction  $f$  of individuals in a population that actually use the app. Fairly high values of  $f$  (of the order of 60%) are required for the digital CT protocol to lead to global protection [2, 9, 23]. These values are in striking contrast with the low app adoption rates observed so far in most countries [30–32].

In this paper we take a different approach. We compare the effectiveness of the two CT protocols in exactly the same conditions, i.e., in the very same realistic epidemiological scenario, without making claims on their absolute performance, and we estimate their relative contribution in realistic hybrid protocols, where the two strategies are complementary. We consider a sensible epidemiological model incorporating all main ingredients of the current epidemic, with parameters tuned to values derived from empirical observations about COVID-19 spreading. Within this single framework we consider the impact of both manual and digital CT strategies, working in similar manner but with their own specific features: delayed isolation of contacts, limited scalability and imperfect recall for the manual procedure; dependence on the predetermined app adoption decision for the digital CT.

The comparison reveals that even when the number of reconstructed contacts is the same, manual CT performs better than digital CT in practically all realistic cases. The manual protocol is more efficient in increasing the epidemic threshold (i.e., the value of the effective infection rate above which the infection spreads diffusely), in limiting the height of the epidemic peaks and in reducing the number of isolated individuals. This surprising result is due to the stochastic *annealed* nature of the manual CT procedure, in which each symptomatic node randomly recalls a fraction of her contacts, in contrast with the digital CT where the traced nodes belong deterministically to the prearranged *quenched* fraction of the population adopting the app. In the latter case, the individuals not adopting the app can never be reached by the CT protocol, while the entire population is potentially detectable through the stochastic sampling of the manual procedure. The better performance of manual CT is already evident in homogeneous populations and it is strongly enhanced in the presence of a heterogeneous distribution of contacts. Superspreaders not adopting the app are invisible

to the digital tracing while they are very likely to be detected by a manual tracing originating from one of their many contacts. In a realistic setup where both protocols are adopted simultaneously, manual CT leads to a considerable reduction of the transmission even considering delays and scalability, while the digital protocol produces a relevant contribution only for large adoption rates, as suggested by previous literature.

## II. RESULTS

### A. Epidemic spreading on heterogeneous dynamical networks

We consider an activity-driven network model with attractiveness, taking into account both the temporal dynamics of social contacts and the heterogeneity in the propensity to establish social ties [33–36]. Each susceptible node  $S$  is assigned with an activity  $a_S$  and an attractiveness parameter  $b_S$ , drawn from the joint distribution  $\rho(a_S, b_S)$ : the activation rate  $a_S$  describes the Poissonian activation dynamics of the node; the attractiveness  $b_S$  sets the probability  $p_{b_S} \propto b_S$  for a node to be contacted by an active agent. At the beginning all nodes are disconnected and when a node activates it creates  $m$  links with  $m$  randomly selected nodes (hereafter we set  $m = 1$ ); then all links are destroyed and the procedure is iterated. The functional form of  $\rho(a_S, b_S)$  encodes the correlations between activity and attractiveness in a population with a given distribution of activity. It has been observed that several social systems feature positive correlations between activity and attractiveness and a broad power-law distribution of activity [33–39]:

$$\rho(a_S, b_S) \sim a_S^{-(\nu+1)} \delta(b_S - a_S) \quad (1)$$

with  $\nu$  typically ranging between 0.5 and 2.

On top of the activity-driven dynamics, we consider a compartmental epidemic model which includes the main phases of clinical progression of the SARS-CoV-2 infection [6, 40–42], also applicable to other infectious diseases with asymptomatic and presymptomatic transmission. The model is composed by five compartments:  $S$  susceptible,  $P$  presymptomatic,  $A$  infected asymptomatic,  $I$  infected symptomatic,  $R$  recovered. A contagion process (see Fig. 1a) occurs with probability  $\lambda$  when a link is established between an infected (either  $P$ ,  $A$  and  $I$ ) and a susceptible node  $S$  (contact-driven transition): a node has probability  $\delta$  to become presymptomatic after infection and probability  $(1 - \delta)$  to become asymptomatic, thus  $S \xrightarrow{\lambda\delta} P$  and  $S \xrightarrow{\lambda(1-\delta)} A$ . A presymptomatic node spontaneously develops symptoms with rate  $\gamma_P = 1/\tau_P$ , thus with a Poissonian process  $P \xrightarrow{\gamma_P} I$ ; both asymptomatic and symptomatic nodes spontaneously recover respectively with rate  $\mu = 1/\tau$  and with rate  $\mu_I = \mu\gamma_P/(\gamma_P - \mu)$ , so that the average infectious period for both symptomatic and asymptomatic

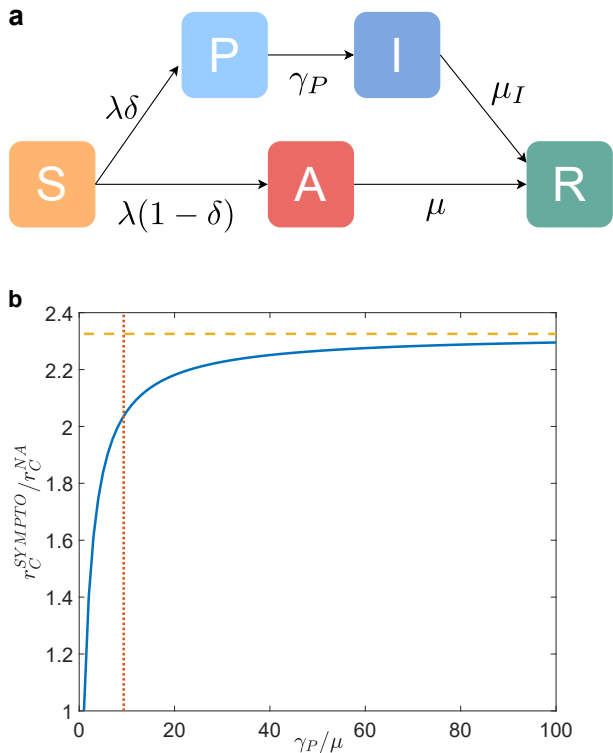


FIG. 1: **Epidemic model without contact tracing.** **a** Diagram of the compartmental epidemic model without CT. **b** We plot, as a function of  $\gamma_P/\mu$ , the ratio between the epidemic threshold  $r_C^{SYMPTO}$  when symptomatic nodes are isolated and the epidemic threshold of the non-adaptive case  $r_C^{NA}$ . The horizontal dashed orange line indicates the value of  $r_C^{SYMPTO}/r_C^{NA}$  for  $\gamma_P = \infty$  (instantaneous onset of symptoms). The vertical red dash-dotted line indicates the value of  $\gamma_P/\mu$  we consider in the rest of the paper. We set  $\rho(a_S, b_S) = \rho_S(a_S)\delta(b_S - a_S)$ . The curve does not depend on the specific form of  $\rho_S(a_S)$ .

is  $\tau$ . We neglect states of hospitalization and consider recovery without death: this choice does not affect the infection dynamics.

Adaptive behavior of populations exposed to epidemics can be modelled within the activity-driven network framework: infected nodes experience a reduction in activity, due to isolation or the appearance of symptoms; similarly, other individuals undertake self-protective behavior to reduce the probability of contact with an infected node, and this is modelled as a reduction in the attractiveness of infected nodes [43–45]. We assume that symptomatic infected nodes  $I$  are immediately isolated ( $a_I, b_I$ ) = (0, 0), therefore not being able to infect anymore. On the contrary, we assume that recovered  $R$ , asymptomatic  $A$  and presymptomatic  $P$  individuals behave as when they were susceptible ( $a_A, b_A$ ) = ( $a_P, b_P$ ) = ( $a_R, b_R$ ) = ( $a_S, b_S$ ). The adaptive behavior is implemented without affecting the activity of nodes which are not isolated [44].

The control parameter  $r = \lambda/\mu$  is the effective infection rate, whose critical value  $r_C$  – the epidemic threshold

– sets the transition point between the absorbing and the active phase of the epidemic. The increase in the value of  $r_C$  is an indicator of the effectiveness of mitigation strategies. Within the adaptive activity-driven framework, the epidemic threshold can be calculated analytically via a mean-field approach (see Methods).

The effect of isolating symptomatic nodes as the only containment measure is shown in Fig. 1b. We compare the epidemic threshold  $r_C$ , obtained with the isolation of symptomatic nodes only, with the epidemic threshold  $r_C^{NA}$  of the non-adaptive (NA) case, in which no containment measures are taken on infected individuals, as a function of  $\gamma_P/\mu$  (see Methods for the explicit expression). In the case of instantaneous symptoms development ( $\gamma_P/\mu \rightarrow \infty$ ), the threshold is increased by a factor of  $1/(1 - \delta)$ , while for smaller  $\gamma_P/\mu$  the gain is reduced. For example, for  $(1 - \delta) = 0.43$ , that is 43% of asymptomatic individuals,  $\tau_P = 1.5$  days and  $\tau = 14$  days as observed for SARS-CoV-2 (see Methods for details on the parameters used in all figures), the threshold is doubled by the isolation of symptomatic nodes. This is the baseline reference for the evaluation of the performance of CT strategies.

## B. Manual and digital contact tracing protocols

The CT protocols differ in their practical implementation as well in their exploration properties.

Manual tracing is performed by personnel who, through interviews, collects information, contacts individuals who may have been infected and arranges for testing. In manual CT, as soon as an individual develops symptoms (i.e.  $P \rightarrow I$ ), her contacts in the previous  $T_{CT}$  days are traced with recall probability  $\varepsilon(a_S)$ , where  $a_S$  is the activity of the symptomatic individual. A traced contact is tested and, if found in state  $A$  (infected asymptomatic), isolated ( $a = b = 0$ ): the average time between the isolation of the symptomatic individual and the isolation of her asymptomatic infected contacts is  $\tau_C$ . Such delay can be quite large, due to the time required for the collection of the diary, the execution of the diagnostic test and the subsequent isolation [2, 17]. Moreover, the manual protocol depends on  $\varepsilon(a_S)$ , which takes into account the limited resources allocated for tracing and the limited memory/knowledge of symptomatic individuals in reconstructing their contacts. Low activity nodes make few contacts over time and a fraction of their contacts will be traced; on the other hand high activity nodes will only remember a finite number of their contacts so that, also because of limitations of the tracing capacity, we expect that at most a number  $k_c$  of contacts can be traced [46, 47]. This translates into the limited scalability property:

$$\varepsilon(a_S) = \begin{cases} \varepsilon^*, & \text{if } a_S \leq a^* \\ \varepsilon^* \frac{a^*}{a_S} = \frac{k_c}{2T_{CT}a_S}, & \text{if } a_S > a^* \end{cases} \quad (2)$$

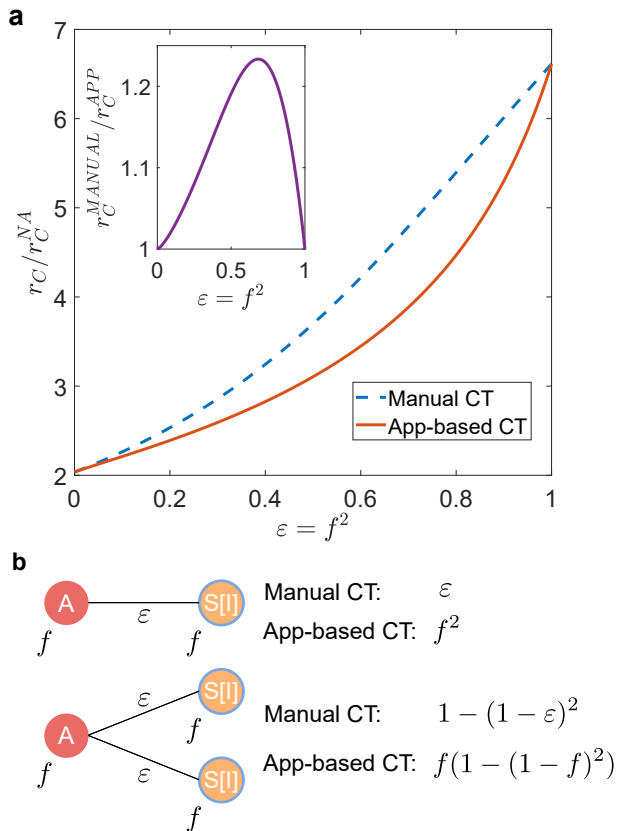


FIG. 2: **Stochastic vs. prearranged sampling in contact tracing.** **a** Plot, as a function of  $\epsilon = f^2$ , of the ratio between the epidemic threshold  $r_C$  in the presence of CT protocols and the epidemic threshold of the non-adaptive case  $r_C^{NA}$ . In the inset we plot the ratio between the epidemic threshold of the manual CT  $r_C^{MANUAL}$  and that of the app-based CT  $r_C^{APP}$ , as a function of  $\epsilon = f^2$ . We consider homogeneous activity and attractiveness, setting  $\rho(a_S, b_S) = \delta(a_S - a)\delta(b_S - b)$ . **b** If an asymptomatic node  $A$  infects a single susceptible node  $S$  (which subsequently becomes symptomatic,  $I$ ), the infector is traced with probability  $\epsilon$  in the manual CT and with probability  $f^2$  in the digital CT. Thus the probability is the same if we impose  $f^2 = \epsilon$ . However, if an asymptomatic node infects two susceptible nodes (which subsequently become symptomatic), the probability of tracing the infector with the manual protocol is  $1 - (1 - \epsilon)^2 = 2f^2 - f^4$  (still considering  $\epsilon = f^2$ ). This value is always larger than that of the digital protocol  $f(1 - (1 - f)^2) = 2f^2 - f^3$ .

where  $a^* = k_c / 2T_{CT}\epsilon^*$ . Manual CT also suffers from a global scalability limitation. Indeed in the active phase with a large number of infected individuals, the tracing system could be ineffective due to the excessive number of contacts to be followed. However, here we focus on the epidemic threshold and we evaluate the features of the CT procedure that keep the epidemic spreading under control before widespread diffusion occurs.

Digital CT is based on the download of an app which allows the tracing of close contacts equipped with the

same app. We assume that each of the individuals has a probability  $f$  to download the app before the epidemic starts. As soon as an individual develops symptoms (i.e.  $P \rightarrow I$ ), if she downloaded the app, her contacts are traced only if they downloaded the app as well. A traced contact is tested and, if found in state  $A$  (infected asymptomatic), is isolated ( $a = b = 0$ ). The time passing between the isolation of a symptomatic individual and the isolation of her asymptomatic infected contacts is taken to be 0, thus assuming an idealized scenario of instantaneous notification and isolation. We finally consider a more realistic scenario where the two procedures are combined into a hybrid protocol in which digital CT supports manual CT, potentially reaching individuals not traced manually [19, 25, 29]. See Methods for details on the implementation of the CT protocols.

### C. Stochastic vs. prearranged sampling

We first compare the manual and digital CT protocols in the case of a population with homogeneous activity and attractiveness,  $\rho(a_S, b_S) = \delta(a_S - a)\delta(b_S - b)$ , without delay even in manual CT, i.e.,  $\tau_C = 0$ . We set  $\epsilon = f^2$  so that the probability that a single contact is traced in the two protocols is the same. However, it should be emphasized that typical values of  $f^2$  range between 0.01 and 0.1 in many countries [30–32], while  $\epsilon$  is usually larger ( $\approx 0.3 - 0.5$ ), since typically 30%–50% of contacts are close and occur at home, at work or at school and thus are easily traceable [48, 49]. An exact analytical estimate of the epidemic threshold is obtained through a linear stability analysis around the absorbing state (see Methods for explicit expressions and Supplementary Method 1 for detailed derivation): in Fig. 2a we compare the threshold for manual and app-based CT, compared to the non-adaptive case (NA), for realistic COVID-19 parameters. Both protocols feature the same epidemic threshold when  $\epsilon = f = 0$  and  $\epsilon = f = 1$ : indeed the former corresponds to the isolation of symptomatic individuals only, without CT, while the latter limit corresponds to the case in which all contacts are traced. For intermediates values of  $\epsilon = f^2$ , manual tracing is strongly and surprisingly more effective than digital tracing, as it increases significantly the epidemic threshold, compared to the app-based protocol. Since we are considering no heterogeneity or delays, the difference is due only to sampling effects in the CT dynamics. In practice, in app-based CT the population to be tested is prearranged, based on whether or not the app was downloaded before the outbreak started. On the contrary, manual CT performs a stochastic sampling of the population: the random exploration can potentially reach the entire population, since anyone who has come in contact with a symptomatic node can be traced. The simplest example of the difference in tracing multiple infections processes in the two protocols is illustrated in Fig. 2b.

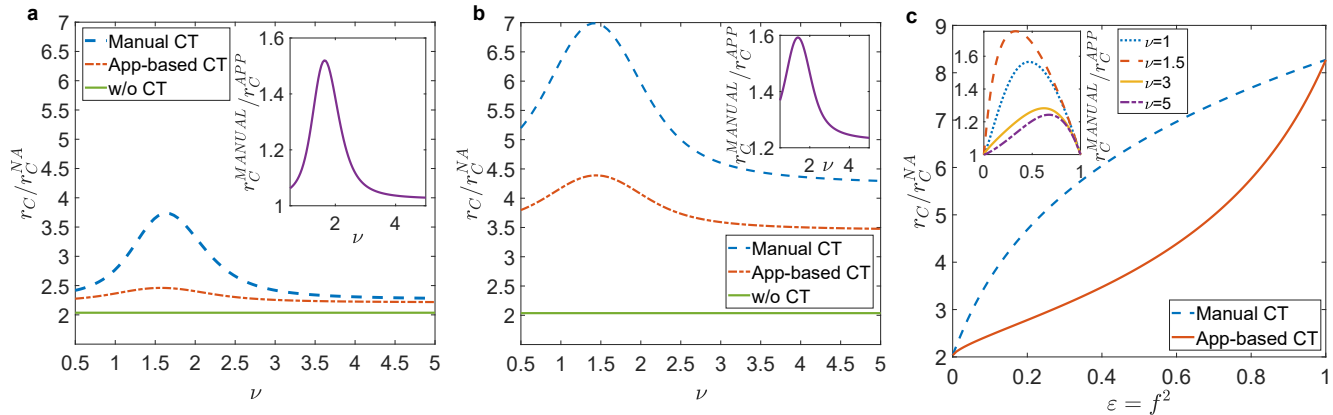


FIG. 3: **Effects of heterogeneity.** **a** Plot, as a function of the exponent  $\nu$ , of the ratio between the epidemic threshold  $r_C$  in the presence of CT protocols and the epidemic threshold of the non-adaptive case  $r_C^{NA}$ . We set  $\varepsilon = f^2 = 0.1$  ( $f \approx 0.316$ ). In the inset we plot the ratio between the epidemic threshold of the manual CT  $r_C^{MANUAL}$  and that of the app-based CT  $r_C^{APP}$ , as a function of  $\nu$ . **b** Same plot as **a** with  $\varepsilon = f^2 = 0.6$  ( $f \approx 0.775$ ). **c** The ratio  $r_C/r_C^{NA}$  is plotted as a function of  $\varepsilon = f^2$  for both CT protocols, with  $\nu = 1.5$ . In the inset we plot the ratio  $r_C^{MANUAL}/r_C^{APP}$  as a function of  $\varepsilon = f^2$  for several  $\nu$  values. In all panels the distribution  $\rho(a_S, b_S)$  is given by Eq. (1).

#### D. Effects of heterogeneous activity

We now consider a heterogeneous activity distribution, as observed in several human systems, and we consider a positive activity-attractiveness correlation, as defined in Eq. (1) [33–35, 37–39]. The power-law distribution for the activity implies the presence of hubs with high activity and high attractiveness. We investigate the pure effect of heterogeneities in contact tracing [12, 27] setting now  $\varepsilon(a_S) = \varepsilon$ ,  $\forall a_S$  and not considering delays in manual CT,  $\tau_C = 0$ . We perform again a mean-field approach, obtaining an analytical closed form for the epidemic threshold (see Methods and Supplementary Method 1): in Fig. 3 we compare the epidemic threshold with the two protocols as a function of the exponent  $\nu$  of the activity distribution, for realistic parameters and setting an average activity  $\bar{a}_S = 6.7$  days $^{-1}$  [43, 48]. Both protocols are more effective in heterogeneous populations, that is at  $\nu \sim 1 - 1.5$ . Note that due to the cut-offs and the constraint on the average, the fluctuations of the activity distribution are maximum for  $\nu = 1$ , and the epidemic thresholds depend both on activity fluctuations and higher order moments of  $\rho_S(a_S)$  (see Methods and Supplementary Method 1 for details). However heterogeneity greatly amplifies stochastic effects, further increasing the advantage of the manual tracing over the app-based prearranged protocol. Indeed, in heterogeneous populations nodes with high activity and attractiveness (super-spreaders) drive and sustain the spread of the epidemic. Manual CT is far more effective in identifying and isolating them than app-based CT: in digital CT, hubs which have not downloaded the app will never be traced, despite the high number of their contacts. On the contrary, manual CT is very effective in tracing super-spreaders, because they are engaged in many contacts

and are traced very effectively by stochastic exploration.

#### E. Limited scalability and delay in manual contact tracing

We now consider some features of manual CT that can reduce its effectiveness: the limited scalability of the tracing capacity [46, 47] and the delays in CT and isolation [2, 23, 28]. We set  $\varepsilon(a_S)$  as in Eq. (2) and consider a large delay  $\tau_C = 3$  days [2] in manual CT. In Fig. 4 we compare the epidemic threshold for the two CT protocols, setting equal probabilities of tracing a contact  $\bar{\varepsilon} = f^2$ , where  $\bar{\varepsilon} = \int da_S \varepsilon(a_S) \rho_S(a_S)$ . For small values of  $\bar{\varepsilon}$  (note that this however corresponds to a quite large adoption rate  $f = \sqrt{\bar{\varepsilon}} \approx 0.316$ ) manual CT is still more effective (see Fig. 4a): the delay in isolation and the limited scalability are not able to significantly reduce the advantage provided by the stochastic exploration of contacts. Fig. 4b shows that digital CT can become more effective than manual CT, but this occurs only for very large values of  $f^2$  and  $\tau_C$ . This indicates that for realistic settings, the advantage of the manual protocol over the app-based protocol is robust even including delays and limited scalability. Fig. 4c further illustrates for which (unrealistically large) values of  $f^2$  and  $\tau_C$ , digital CT outperforms manual CT. Note that realistic values of  $f$  correspond to  $f^2$  at most of the order of 0.1. Hence, an extremely high adoption of the app is necessary in order to obtain an effective advantage of the digital CT.

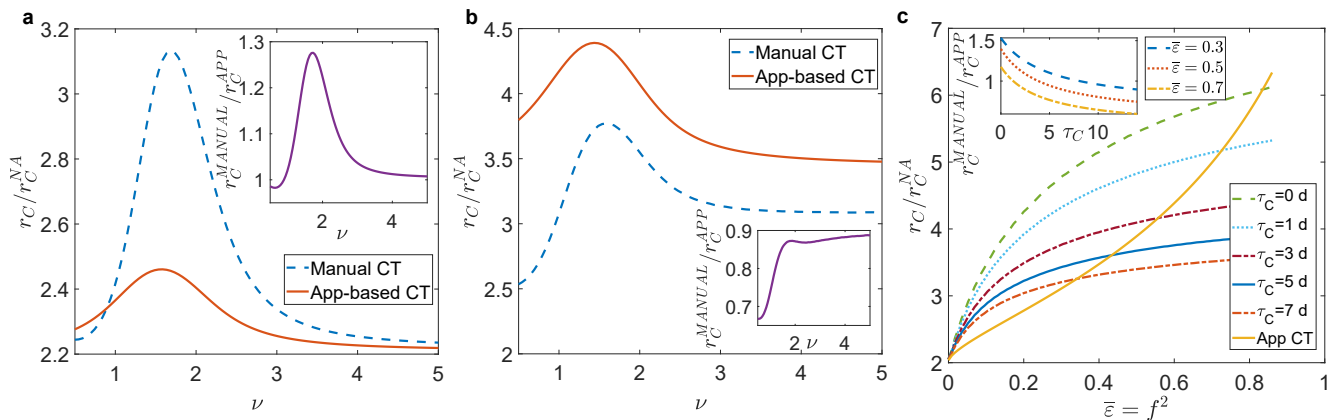


FIG. 4: **Effects of limited scalability and isolation delay in manual contact tracing.** **a** Plot, as a function of the exponent  $\nu$ , of the ratio between the epidemic threshold  $r_C$  in the presence of CT protocols and the epidemic threshold of the non-adaptive case  $r_C^{NA}$ , with limited scalability and delay in manual CT. We set  $\bar{\epsilon} = f^2 = 0.1$  ( $f \approx 0.316$ ),  $\tau_C = 3$  days. In the insets we plot the ratio between the epidemic threshold of the manual CT  $r_C^{MANUAL}$  and that of the app-based CT  $r_C^{APP}$ , as a function of  $\nu$ . **b** Same plot as **a** with  $\bar{\epsilon} = f^2 = 0.6$  ( $f \approx 0.775$ ),  $\tau_C = 5$  days. **c** Plot of the ratio  $r_C/r_C^{NA}$  as a function of  $\bar{\epsilon} = f^2$  for both CT protocols, setting  $\nu = 1.5$  and for several values of  $\tau_C$ . In the inset we plot the ratio  $r_C^{MANUAL}/r_C^{APP}$  as a function of  $\tau_C$  for several  $\bar{\epsilon}$  values. In all panels the distribution  $\rho(a_S, b_S)$  is given by Eq. (1).

### F. Manual and app-based CT in the epidemic phase

We now explore with numerical simulations (see Methods, Supplementary Method 2) the effects of manual and digital CT protocols in the active phase of the epidemic. We consider an optimistic value of  $f = 0.316$ , setting  $\bar{\epsilon} = f^2 = 0.1$  that is a very low value for the recall probability, and we consider the system above the epidemic threshold  $r > r_c$ , in the conditions of Fig. 4a. Fig. 5 shows that the infection peak with manual tracing is lower than the app-based one. Moreover, in the manual CT the duration of the epidemic is reduced: this strongly impacts on the final epidemic size, which is about half of the one observed in the app-based CT. We also plot the temporal evolution of the average activity of the system  $\langle a(t) \rangle$  and of the fraction of isolated nodes  $\text{Iso}(t)$  (see inset). In general, the average activity  $\langle a(t) \rangle$  features a minimum, however its value remains very large (about 98% of the case without any tracing measure). This implies that both protocols do not disrupt the functionality of the system. Interestingly, the fraction of isolated nodes is coherent with the infection peak, and in particular it is lower when the infection peak is lowered. This means that the most effective procedure, i.e. manual CT for realistic values of the parameters, not only lowers the infection peak but it is also able to isolate a smaller number of nodes, a key feature of any effective CT strategy.

### G. Robustness

In the Supplementary Notes we show that the advantage of the manual CT is robust with respect to the relaxation of several assumptions and to changes of param-

eters. In particular, we consider the case where all nodes have equal attractiveness  $\rho(a_S, b_S) = \rho_S(a_S)\delta(b_S - b)$ , we take into account very long delays  $\tau_C$  and we change the maximum number of traceable contacts  $k_c$ . We also show that the advantage of manual contact tracing in the presence of heterogeneous activity is robust, if one takes into account that contacts belonging to the close social circle of the index case (same household) are always traced and isolated manually, also in the digital protocol. This can be verified by using a hybrid procedure with a fixed small number of contacts always traced (see Supplementary Notes).

### H. Hybrid contact tracing protocols: manual plus digital CT

We now consider the implementation of a realistic hybrid CT protocol with manual and digital contact tracing working at the same time. We assume that each individual has downloaded the app with probability  $f$  before the epidemic starts. As soon as an individual with activity  $a_S$  develops symptoms (i.e.  $P \rightarrow I$ ), contact tracing is activated with reference to the previous  $T_{CT}$  days: if the infected individual and also her contact downloaded the app, the contacted agent is immediately traced and isolated with no delay. Otherwise, the contact can only be traced manually, with probability  $\epsilon(a_S)$  (as in Eq. (2)) and, if found in state  $A$ , the contact is isolated with a delay  $\tau_C$ . We set a realistically large delay  $\tau_C = 3$  days.

The threshold in the hybrid case can be determined through the solution of a complex set of equations, that we solve numerically in Supplementary Method 1. In the presence of heterogeneous activity (i.e. superspreaders), starting from a purely digital protocol (Fig. 6b,c)

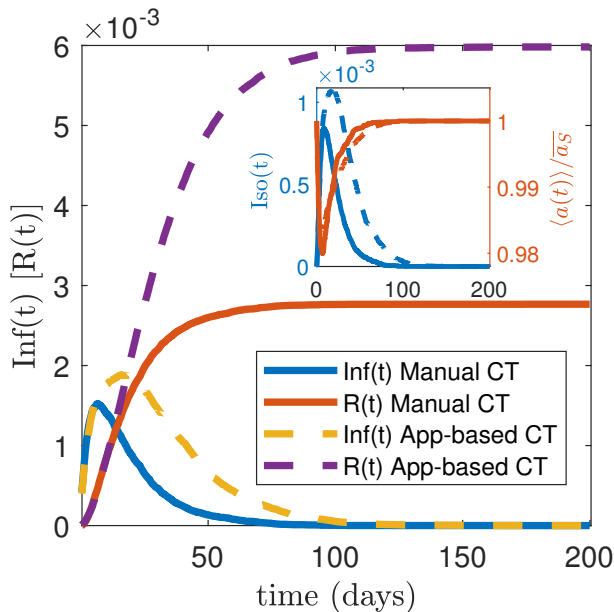


FIG. 5: **Effects of manual and digital contact tracing on the epidemic active phase.** We plot the temporal evolution of the fraction of infected nodes  $\text{Inf}(t)$ , i.e. infected asymptomatic and infected symptomatic, and of the fraction of removed nodes  $R(t)$ , for both manual and digital CT. In the inset we plot the temporal evolution of the fraction of isolated nodes  $\text{Iso}(t)$  (right y-axis) and of the average activity of the population  $\langle a(t) \rangle / \bar{a}_S$  (left y-axis), normalized with  $\bar{a}_S$ . All curves are averaged on several realizations of the disorder and of the temporal evolution. We set  $\bar{\varepsilon} = f^2 = 0.1$ ,  $\tau_C = 3$  days,  $r/r_C^{NA} = 3.1$  and  $N = 5 \cdot 10^3$ . The distribution  $\rho(a_S, b_S)$  is given by Eq. (1), with  $\nu = 1.5$ . The curves for digital and manual CT are averaged respectively over 554 and 681 realizations and the errors, evaluated through the standard deviation, are smaller or comparable with the curves thickness.

the addition of manual contact tracing rapidly increases the threshold, leading to an improvement by a large factor (about 80%), for realistic values  $\bar{\varepsilon} \gtrsim 0.3$ . Instead, starting from a realistic manual contact tracing setup  $\bar{\varepsilon} \gtrsim 0.3$ , a significant improvement (i.e. a 50% of threshold increase) is obtained by implementing a digital contact tracing only if  $f \gtrsim 0.60 - 0.75$  (Fig. 6a,c). These values are consistent with other results in the literature [2, 9, 23]; however, in most countries, the app adoption rates do not reach these values [30–32].

### III. DISCUSSION

Our results indicate that manual CT, despite its drawbacks, can be an efficient protocol in heterogeneous populations, more efficient than its digital counterpart, due to its specific sampling properties. This conclusion is robust with respect to variations in several model assumptions, including correlations between activity and attractiveness or the limited scalability of the manual CT pro-

tol. However, epidemic propagation and strategies to mitigate it are very complex processes and several of their features have been left out from our modelling scheme. Some of these features (the possibility that isolation is non complete, that some individuals do not report symptoms or the existence of testing campaigns detecting infected nonsymptomatic individuals) act similarly on both types of CT and hence do not modify the relative performance. Other more realistic features (the presence of delays even in digital CT and the existence of additional sources of heterogeneity in viral shedding [50], recovery rates [51] and activity temporal patterns [52]) would even reduce the relative performance of digital CT.

Our results put forward several directions to increase the effectiveness of tracing. An important aspect is the correlation between app adoption rates and activity of nodes: our analysis in the Supplementary Notes shows that, as expected, in heterogeneous populations a positive correlation strongly increases the success of digital CT. This is a direction that could be pursued in campaigns aimed at driving app adoption among potential superspreaders. However, this represents a challenge for policy makers. Evidence is currently emerging that those who download the app are individuals who adopt very cautious behavior, i.e.  $f$  and  $a_S$  are typically anticorrelated [53, 54]. Another road that could enhance the efficacy of CT protocols is to follow chains of transmissions along multiple steps, so that when a traced contact is found infected also her contacts are reconstructed and tested. This additional step improves the overall effectiveness of CT protocols, but also increases the delay associated to the manual procedure with respect to the digital one. Digital CT allows in principle to extend the tracing procedure to an arbitrary number of steps, however, strong concerns related to privacy issues [55] make this path difficult to follow.

In summary, even if additional features of CT can be considered, the weakness of digital CT, originated by the nature of the sampling of contacts and worsened by heterogeneities, seems to be an intrinsic unavoidable property of the procedure. The manual CT protocol, with its higher intrinsic stochasticity, does not suffer from this problem and samples contacts effectively, especially in realistic heterogeneous populations: thus, digital CT cannot be considered simply as a cheaper and more rapid way of implementing standard contact tracing and should only be considered in combination with manual protocols. Manual CT must necessarily play an important role in any strategy to mitigate the current pandemic. Considerations about costs and practical feasibility of the two approaches (which have not been taken into account here) suggest that a careful integration of the two protocols may be the key for more effective mitigation strategies. As suggested in the last part of our results, an optimal set up should include both procedures, adopted simultaneously. In this respect, the availability of detailed data about the rates of app adoption in various population groups (and correlations with age or activity

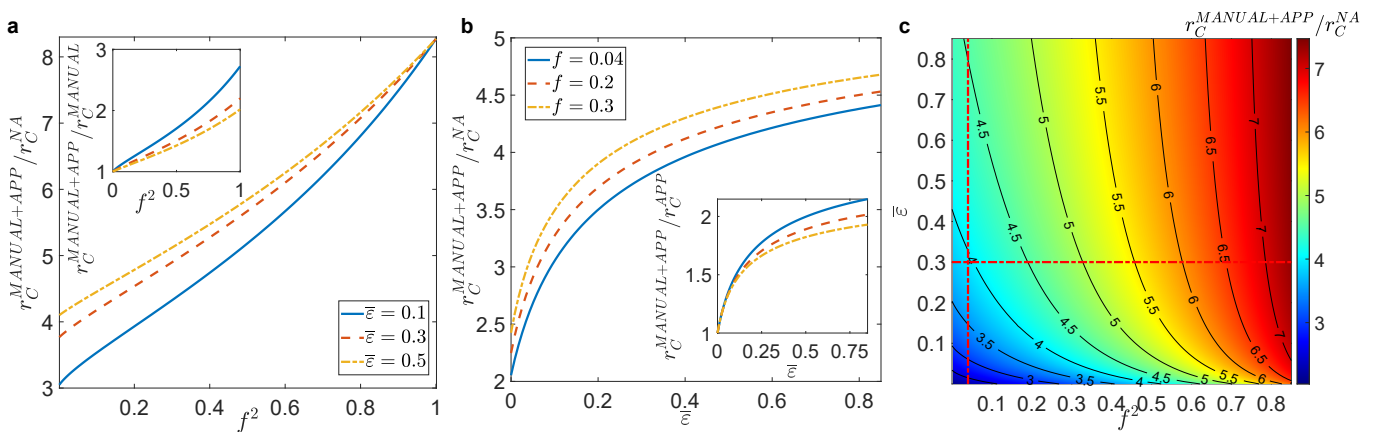


FIG. 6: **Effects of hybrid contact tracing protocol.** **a** Plot, as a function of  $f^2$ , of the ratio between the epidemic threshold in the presence of a hybrid CT protocol,  $r_C^{MANUAL+APP}$ , and the epidemic threshold of the non-adaptive case,  $r_C^{NA}$ , for realistic values of  $\bar{\varepsilon}$  (see legend). In the inset we plot, as a function of  $f^2$ , the ratio between  $r_C^{MANUAL+APP}$  and the epidemic threshold when only manual CT is implemented,  $r_C^{MANUAL}$ . **b** Plot of the ratio  $r_C^{MANUAL+APP}/r_C^{NA}$  as a function of  $\bar{\varepsilon}$ , for realistic app adoption levels  $f$  (see legend). In the inset we plot, as a function of  $\bar{\varepsilon}$ , the ratio between  $r_C^{MANUAL+APP}$  and the epidemic threshold when only app-based CT is implemented,  $r_C^{APP}$ . **c** The ratio  $r_C^{MANUAL+APP}/r_C^{NA}$  is plotted as a function of  $f^2$  and  $\bar{\varepsilon}$ , through a heat map: the red dash-dotted lines are plotted for  $\bar{\varepsilon} = 0.3$  and  $f = 0.2$ , i.e. they correspond to the red dashed curves of panel **a** and **b**. In all panels the distribution  $\rho(a_S, b_S)$  is given by Eq. (1), the manual CT features a delay of  $\tau_C = 3$  days and limited scalability is considered.

levels), as well as more precise estimates of other parameters, such as the recall probability, would be highly beneficial. The design of optimal hybrid CT protocols, including decisions on how to allocate resources and how to target recommendations for app adoption, is a very promising direction for future work.

## IV. METHODS

### A. Mean-field equations and implementation of CT protocols

We consider an activity-attractiveness based mean-field approach, dividing the population into classes of nodes with the same activity  $a_S$  and attractiveness  $b_S$  and treating them as if they were statistically equivalent. For each class  $(a_S, b_S)$  we consider the probability that at time  $t$  a node is in one of the epidemic compartments. For arbitrary  $\rho(a_S, b_S)$  distribution and arbitrary functional form of  $f(a_S)$  and  $\varepsilon(a_S)$  we build the mean-field equations which describe the temporal evolution of the network, the epidemic spreading and the adaptive behavior due to isolation and CT. In particular, in order to model the manual and app-based CT we introduce two further compartments:  $T$  traced asymptomatic and  $Q$  isolated asymptomatic. An asymptomatic individual became traced  $T$  when infected by a presymptomatic node or when she infects a susceptible node that eventually develops symptoms. In the manual case the tracing is effective with probability  $\varepsilon(a)$ . In the app-based case, tracing occurs only if both nodes involved in the con-

tact downloaded the app. A traced node is still infective  $(a_T, b_T) = (a_S, b_S)$  and with rate  $\gamma_A = 1/\tau_A \gg \mu$  it is quarantined,  $T \xrightarrow{\gamma_A} Q$ ; while a quarantined node is no more infective since  $(a_Q, b_Q) = (0, 0)$ . In order to take into account the delay in the manual CT we set:  $\tau_A = \tau_C + \tau_P$  for the manual case and  $\tau_A = \tau_P$  for the app-based process. See Supplementary Method 1 for the detailed equations of manual, digital and hybrid CT protocols.

### B. Epidemic thresholds

We perform a linear stability analysis of the mean field equations around the absorbing state obtaining the conditions for its stability and then the epidemic threshold  $r_C$  (see Supplementary Method 1 for details). For the non-adaptive case (NA), when infected individuals do not modify their behavior, the threshold is equal to the one obtained in Refs. [35, 44]. Indeed, setting  $\rho(a_S, b_S) = \rho_S(a_S)\delta(b_S - a_S)$  we obtain:

$$r_C^{NA} = \frac{\overline{a_S}}{2a_S^2} \quad (3)$$

If only symptomatic nodes are isolated as soon as they develop symptoms, we obtain, setting  $\rho(a_S, b_S) = \rho_S(a_S)\delta(b_S - a_S)$ :

$$r_C^{SYMPTO} = r_C^{NA} \frac{\frac{\gamma_P}{\mu}}{\delta + (1 - \delta)\frac{\gamma_P}{\mu}} \quad (4)$$

For the case with CT on homogeneous population, we set  $\rho(a_S, b_S) = \delta(a_S - a)\delta(b_S - b)$ ,  $\varepsilon(a_S) = \varepsilon$  and no delay

in manual CT  $\tau_C = 0$ . We obtain the epidemic threshold

$$r_C^{MANUAL} = \frac{2r_C^{NA} \frac{\gamma_P}{\mu}}{\delta + (1 - \delta - \varepsilon\delta) \frac{\gamma_P}{\mu} + \sqrt{(\delta + (1 - \delta - \varepsilon\delta) \frac{\gamma_P}{\mu})^2 + 4\delta^2 \varepsilon \frac{\gamma_P}{\mu}}} \quad (5)$$

$$r_C^{APP} = \frac{2r_C^{NA} \frac{\gamma_P}{\mu}}{\delta + (1 - \delta - f\delta) \frac{\gamma_P}{\mu} + \sqrt{(\delta + (1 - \delta - f\delta) \frac{\gamma_P}{\mu})^2 + 4\delta f \frac{\gamma_P}{\mu} (\delta + \frac{\gamma_P}{\mu} (1 - f)(1 - \delta))}} \quad (6)$$

The more general case of populations with arbitrary distribution  $\rho(a_S, b_S)$ , arbitrary delays  $\tau_C$  and general form of  $\varepsilon(a_S)$  and  $f(a_S)$ , is reported in Supplementary Method 1. In Supplementary Method 1 we also report the derivation of the epidemic threshold for the hybrid protocol. Its values are derived from the stability conditions of a complex set of 22 differential equations, that we can solve numerically.

### C. Model parameters

Figures present results where one of the model parameters is varied and all the others are fixed. Here we report the parameter values used throughout the paper, unless specified otherwise. They are tailored to describe the current COVID-19 pandemic.

The fraction of infected individuals who develop symptoms is  $\delta = 0.57$  [1]. The time after which a presymptomatic individual spontaneously develops symptoms is  $\tau_P = 1.5$  days [6, 41, 49], while infected individuals recover on average after  $\tau = 14$  days [42, 50]. The time window over which contacts are reconstructed is  $T_{CT} = 14$  days [49]: it is fixed equal to  $\tau$  to track both nodes infected by the index case in the pre-symptomatic phase (forward CT) and the primary case who infected the index case (backward CT) [12]. The maximum number of contacts engaged in  $T_{CT}$  by a single individual that can be reconstructed with the manual CT procedure is  $k_C = 130$ , according to reasonable estimates of the number of contacts manually traced for very ac-

for both the manual and digital CT:

tive individuals [49]. Moreover, fixing  $k_C = 130$  and for realistic  $\bar{\varepsilon} \sim 0.1 - 0.5$  [48], the average number of traced contacts for each index case is approximatively 10 – 60, consistently with reported data on manual CT and with estimates for resources allocation [46, 49, 56, 57] (see Supplementary Notes for the distribution  $P(k_T)$  of contacts  $k_T$  traced manually by each index case). The activity-driven network parameters are fixed so that the average value of the activity is always the same, i.e.  $\bar{a}_S = 6.7 \text{ days}^{-1}$  [43, 48]. In particular for a power-law distribution  $\rho_S(a_S) \sim a_S^{-(\nu+1)}$ , the values of  $a_S$  are constrained between a minimum and a maximum value ( $a_m < a_S < a_M$ ). We keep  $a_M = 10^3 a_m$  and then we tune  $a_m$  to set  $\bar{a}_S$ .

### D. Numerical simulations

We perform numerical simulations of the epidemic model on the adaptive activity-driven network: the network dynamics and epidemic spreading are implemented by a continuous time Gillespie-like algorithm. We consider an activity-driven network of  $N$  nodes. The results are averaged over several realizations of the disorder and of the dynamical evolution, so that the error on the infection peak height is lower than 6%. The initial conditions are imposed by infecting the node with the highest activity  $a_S$  and the CT protocols are immediately adopted. A detailed description of the simulations is reported in Supplementary Method 2.

- 
- [1] Lavezzo, E. *et al.* Suppression of a sars-cov-2 outbreak in the italian municipality of vo'. *Nature* **584**, 425–429 (2020).
- [2] Ferretti, L. *et al.* Quantifying sars-cov-2 transmission suggests epidemic control with digital contact tracing. *Science* **368**, eabb6936 (2020).
- [3] Rothe, C. *et al.* Transmission of 2019-ncov infection from an asymptomatic contact in germany. *N. Engl. J. Med.*

- 382**, 970–971 (2020).
- [4] Pinotti, F. *et al.* Tracing and analysis of 288 early sars-cov-2 infections outside china: A modeling study. *PLOS Med.* **17**, 1–13 (2020).
- [5] Li, R. *et al.* Substantial undocumented infection facilitates the rapid dissemination of novel coronavirus (sars-cov-2). *Science* **368**, 489–493 (2020).
- [6] Wei, W. E. *et al.* Presymptomatic transmission of sars-

- cov-2—singapore, january 23–march 16, 2020. *Morb. Mortal. Wkly. Rep.* **69**, 411 (2020).
- [7] Bonaccorsi, G. *et al.* Economic and social consequences of human mobility restrictions under covid-19. *Proc. Natl. Acad. Sci. U.S.A.* **117**, 15530–15535 (2020).
- [8] Nicola, M. *et al.* The socio-economic implications of the coronavirus pandemic (covid-19): A review. *Int. J. Surg.* **78**, 185 – 193 (2020).
- [9] Eames, K. T. & Keeling, M. J. Contact tracing and disease control. *Proc. Royal Soc. B* **270**, 2565–2571 (2003).
- [10] Fraser, C., Riley, S., Anderson, R. M. & Ferguson, N. M. Factors that make an infectious disease outbreak controllable. *Proc. Natl. Acad. Sci. U.S.A.* **101**, 6146–6151 (2004).
- [11] Klinkenberg, D., Fraser, C. & Heesterbeek, H. The effectiveness of contact tracing in emerging epidemics. *PLOS ONE* **1**, 1–7 (2006).
- [12] Kojaku, S., Hébert-Dufresne, L., Mones, E., Lehmann, S. & Ahn, Y.-Y. The effectiveness of backward contact tracing in networks. *Nat. Phys.* <https://doi.org/10.1038/s41567-021-01187-2> (2021).
- [13] McLean, E. *et al.* Pandemic (h1n1) 2009 influenza in the uk: clinical and epidemiological findings from the first few hundred (ff100) cases. *Epidemiol. Infect.* **138**, 1531–1541 (2010).
- [14] Crook, P. *et al.* Lack of secondary transmission of ebola virus from healthcare worker to 238 contacts, united kingdom, december 2014. *Emerg. Infect. Dis.* **23**, 2081 (2017).
- [15] Bell, D. M., on International, W. H. O. W. G. & of SARS, C. T. Public health interventions and sars spread, 2003. *Emerg. Infect. Dis.* **10**, 1900–1906 (2004).
- [16] Wilder-Smith, A., Chiew, C. J. & Lee, V. J. Can we contain the covid-19 outbreak with the same measures as for sars? *Lancet Infect. Dis.* **20**, e102–e107 (2020).
- [17] Hellewell, J. *et al.* Feasibility of controlling covid-19 outbreaks by isolation of cases and contacts. *Lancet Glob. Health* **8**, e488 – e496 (2020).
- [18] Privacy-preserving contact tracing. <https://covid19.apple.com/contacttracing> (2020).
- [19] Troncoso, C. *et al.* Decentralized privacy-preserving proximity tracing. *IEEE Data Eng. Bull.* **43**, 36–66 (2020).
- [20] Oliver, N. *et al.* Mobile phone data for informing public health actions across the covid-19 pandemic life cycle. *Sci. Adv.* **6**, eabc0764 (2020).
- [21] Ahmed, N. *et al.* A survey of covid-19 contact tracing apps. *IEEE Access* **8**, 134577–134601 (2020).
- [22] Sapiezynski, P., Pruessing, J. & Sekara, V. The fallibility of contact-tracing apps. Preprint at <https://arxiv.org/abs/2005.11297> (2020)
- [23] Braithwaite, I., Callender, T., Bullock, M. & Aldridge, R. W. Automated and partly automated contact tracing: a systematic review to inform the control of covid-19. *Lancet Digital Health* **2**, e607–e621 (2020).
- [24] Zastrow, M. Coronavirus contact-tracing apps: can they slow the spread of covid-19? *Nature - Technology Feature* <https://doi.org/10.1038/d41586-020-01514-2> (19 May 2020).
- [25] Cencetti, G. *et al.* Digital proximity tracing on empirical contact networks for pandemic control. *Nat. Commun.* **12**, 1655 (2021).
- [26] Almagor, J. & Picascia, S. Exploring the effectiveness of a covid-19 contact tracing app using an agent-based model. *Sci. Rep.* **10**, 22235 (2020).
- [27] Nielsen, B. F., Sneppen, K., Simonsen, L. & Mathiesen, J. Social network heterogeneity is essential for contact tracing. Preprint at <https://doi.org/10.1101/2020.06.05.20123141> (2020)
- [28] Kretzschmar, M. E. *et al.* Impact of delays on effectiveness of contact tracing strategies for covid-19: a modelling study. *Lancet Public Health* **5**, e452 – e459 (2020).
- [29] Barrat, A., Cattuto, C., Kivela, M., Lehmann, S. & Saramäki, J. Effect of manual and digital contact tracing on covid-19 outbreaks: a study on empirical contact data. Preprint at <https://doi.org/10.1101/2020.07.24.20159947> (2020)
- [30] Alessandro, L. Immuni è efficace? gli ultimi numeri, le luci e le ombre dell’app per il covid-19. *Sole24Ore* (2020). 09-09-2020.
- [31] O’Neill, P. H., Ryan-Mosley & Johnson, B. A flood of coronavirus apps are tracking us. now it’s time to keep track of them. *MIT Technology Review* (2020). Tech policy/Privacy: 09-29-2020.
- [32] MIT Technology Review. Covid tracing tracker. [https://docs.google.com/spreadsheets/d/1ATaIAS08KtZMx\\_zJREoOvFhOnmB-sAqJ1-CjVRSC0w/edit#gid=0](https://docs.google.com/spreadsheets/d/1ATaIAS08KtZMx_zJREoOvFhOnmB-sAqJ1-CjVRSC0w/edit#gid=0) (2020). Accessed on: 09-29-2020.
- [33] Perra, N., Gonçalves, B., Pastor-Satorras, R. & Vespignani, A. Activity driven modeling of time varying networks. *Sci. Rep.* **2**, 469 (2012).
- [34] Ubaldi, E. *et al.* Asymptotic theory of time-varying social networks with heterogeneous activity and tie allocation. *Sci. Rep.* **6**, 35724 (2016).
- [35] Pozzana, I., Sun, K. & Perra, N. Epidemic spreading on activity-driven networks with attractiveness. *Phys. Rev. E* **96**, 042310 (2017).
- [36] Tizzani, M. *et al.* Epidemic spreading and aging in temporal networks with memory. *Phys. Rev. E* **98**, 062315 (2018).
- [37] Ghoshal, G. & Holme, P. Attractiveness and activity in internet communities. *Physica A* **364**, 603 – 609 (2006).
- [38] Ubaldi, E., Vezzani, A., Karsai, M., Perra, N. & Burioni, R. Burstiness and tie activation strategies in time-varying social networks. *Sci. Rep.* **7**, 46225 (2017).
- [39] Starnini, M., Baronchelli, A. & Pastor-Satorras, R. Modeling human dynamics of face-to-face interaction networks. *Phys. Rev. Lett.* **110**, 168701 (2013).
- [40] Guan, W.-j. *et al.* Clinical characteristics of coronavirus disease 2019 in china. *N. Engl. J. Med.* **382**, 1708–1720 (2020).
- [41] Di Domenico, L., Pullano, G., Sabbatini, C. E., Boëlle, P.-Y. & Colizza, V. Impact of lockdown on covid-19 epidemic in île-de-france and possible exit strategies. *BMC Med.* **18**, 240 (2020).
- [42] World Health Organization. Report of the who-china joint mission on coronavirus disease 2019 (covid-19). <https://www.who.int/docs/default-source/coronaviruse/who-china-joint-mission-on-covid-19-final-report.pdf> (2020). Accessed on: 09-29-2020.
- [43] Van Kerckhove, K., Hens, N., Edmunds, W. J. & Eames, K. T. D. The Impact of Illness on Social Networks: Implications for Transmission and Control of Influenza. *Am. J. Epidemiol.* **178**, 1655–1662 (2013).
- [44] Mancastropa, M., Burioni, R., Colizza, V. & Vezzani, A. Active and inactive quarantine in epidemic spreading on adaptive activity-driven networks. *Phys. Rev. E* **102**,

- 020301 (2020).
- [45] Fenichel, E. P. *et al.* Adaptive human behavior in epidemiological models. *Proc. Natl. Acad. Sci. U.S.A.* **108**, 6306–6311 (2011).
- [46] European Center for Disease Prevention and Control. Resource estimation for contact tracing, quarantine and monitoring activities for covid-19 cases in the eu/eea. <https://www.ecdc.europa.eu/sites/default/files/documents/COVID-19-resources-for-contact-tracing-2-March-2020.pdf> (2020). Accessed on: 09-29-2020.
- [47] Centers for Disease Control and Prevention. Scaling up staffing roles in case investigation and contact tracing. <https://www.cdc.gov/coronavirus/2019-ncov/php/contact-tracing/contact-tracing-plan/scaling-staff.html> (2020). Accessed on: 09-29-2020.
- [48] Mossong, J. *et al.* Social contacts and mixing patterns relevant to the spread of infectious diseases. *PLOS Med.* **5**, 1–1 (2008).
- [49] Keeling, M. J., Hollingsworth, T. D. & Read, J. M. Efficacy of contact tracing for the containment of the 2019 novel coronavirus (covid-19). *J. Epidemiology Community Health* **74**, 861–866 (2020).
- [50] Liu, Y. *et al.* Viral dynamics in mild and severe cases of covid-19. *Lancet Infect. Dis.* **20**, 656–657 (2020).
- [51] de Arruda, G. F., Petri, G., Rodrigues, F. A. & Moreno, Y. Impact of the distribution of recovery rates on disease spreading in complex networks. *Phys. Rev. Res.* **2**, 013046 (2020).
- [52] Mancastropa, M., Vezzani, A., Muñoz, M. A. & Buri-  
oni, R. Burstiness in activity-driven networks and the epidemic threshold. *J. Stat. Mech. Theory Exp.* **2019**, 053502 (2019).
- [53] von Wyl, V. *et al.* Drivers of acceptance of covid-19 proximity tracing apps in Switzerland: panel survey analysis. *JMIR Public Health Surveill.* **7**, e25701 (2021).
- [54] Saw, Y. E., Tan, E. Y., Liu, J. S. & Liu, J. C. Predicting public uptake of digital contact tracing during the covid-19 pandemic: results from a nationwide survey in Singapore. *J. Med. Internet Res.* **23**, e24730 (2021).
- [55] Firth, J. A. *et al.* Using a real-world network to model localized covid-19 control strategies. *Nat. Med.* **26**, 1616–1622 (2020).
- [56] European Center for Disease Prevention and Control. Contact tracing for covid-19: current evidence, options for scale-up and an assessment of resources needed. <https://www.ecdc.europa.eu/sites/default/files/documents/COVID-19-Contract-tracing-scale-up.pdf> (2020). Accessed on: 09-29-2020.
- [57] Visontay, E. Victoria’s contact-tracing effort buckles under the weight of covid-19 cases. *The Guardian* (2020). 08-04-2020.

# Supplementary Information for ”Stochastic sampling effects favor manual over digital contact tracing”

Marco Mancastroppa and Raffaella Burioni

*Dipartimento di Scienze Matematiche, Fisiche e Informatiche,  
Università degli Studi di Parma, Parco Area delle Scienze, 7/A 43124 Parma, Italy and  
INFN, Sezione di Milano Bicocca, Gruppo Collegato di Parma,  
Parco Area delle Scienze, 7/A 43124 Parma, Italy*

Claudio Castellano

*Istituto dei Sistemi Complessi (ISC-CNR), Via dei Taurini 19, I-00185 Roma, Italy*

Alessandro Vezzani

*Istituto dei Materiali per l'Elettronica ed il Magnetismo (IMEM-CNR),  
Parco Area delle Scienze, 37/A-43124 Parma, Italy and  
Dipartimento di Scienze Matematiche, Fisiche e Informatiche,  
Università degli Studi di Parma, Parco Area delle Scienze, 7/A 43124 Parma, Italy*

## Contents

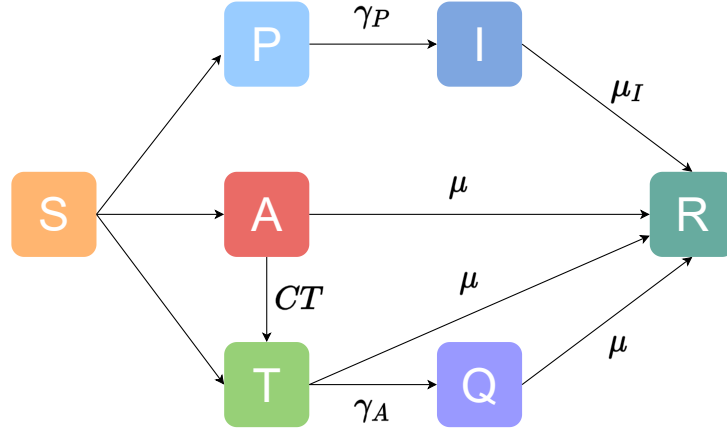
<b>I. Supplementary Method 1: Mean-field equations and analytical derivation of the epidemic thresholds</b>	<b>1</b>
A. Manual CT	2
B. Digital CT	5
C. Hybrid CT	9
D. Limit cases	11
1. Non-adaptive case (NA)	11
2. Isolation of only symptomatic nodes	11
3. Homogeneous case without delays and without limited scalability	12
4. Heterogeneous case	12
<b>II. Supplementary Method 2: Continuous time Gillespie-like algorithm for network dynamics and epidemic evolution</b>	<b>13</b>
<b>III. Supplementary Notes: Robustness of the results</b>	<b>14</b>
A. Activity-attractiveness distribution, limited scalability parameters and delays	14
B. Epidemic active phase	14
C. Deterministic household CT	15
D. Correlation between probability of app adoption and individual activity	16

In this supplementary information we derive the mean-field equations for the temporal evolution of the epidemic model on adaptive activity-driven networks. We also derive analytically the epidemic threshold and we describe the scheme of the continuous-time Gillespie-like algorithm used for the numerical approach to the temporal evolution of the network and of the epidemic. Finally, we discuss in detail the robustness of the results, relaxing assumptions in activity distribution, changing most CT parameters in the modelling scheme, introducing further realistic features such as deterministic household CT and correlation between app adoption and individual activity.

## I. Supplementary Method 1: Mean-field equations and analytical derivation of the epidemic thresholds

We consider the epidemic model proposed in the main text evolving on an adaptive activity-driven network in the presence of contact tracing of asymptomatic nodes.

The epidemic model proposed is a Susceptible-Infected-Recovered (SIR) model, with a further distinction for the states of infection  $I$ . The distinction is based on the presence of symptoms, on tracing and isolation and it models changes in social behaviour depending on nodes' health status. We do not consider here burstiness effects [1] nor memory [2].



Supplementary Fig. 1: **Epidemic model with contact tracing.** We plot the scheme of the epidemic model with the transitions for CT. The rates for the infection events (emanating from  $S$ ) and for the CT events are not indicated, as the relevant events, indicated in the text, are complicated.

## A. Manual CT

We first focus on the manual CT. In the original epidemic model, individuals can be in states  $S$  (susceptible),  $P$  (infected presymptomatic),  $I$  (infected symptomatic),  $A$  (infected asymptomatic) and  $R$  (recovered). In the presence of CT, two additional compartments appear:  $T$  (asymptomatic traced) and  $Q$  (asymptomatic quarantined). The possible transitions among these states are depicted in Supplementary Fig. 1.

There are two types of events related to CT: an asymptomatic individual  $A$  becomes traced  $T$  when infected by a presymptomatic node  $P$  (forward CT) or when she infects a susceptible node that eventually develops symptoms (backward CT). A traced individual remains infectious  $(a_T, b_T) = (a_S, b_S)$  until the presymptomatic starts developing symptoms. Only after that moment she enters quarantine  $(a_Q, b_Q) = (0, 0)$ . For this reason, the rate for the transition  $T \rightarrow Q$  is  $\gamma_A = 1/\tau_A$ , with  $\tau_A = \tau_P + \tau_C$ , where  $\tau_P = 1/\gamma_P$  and  $\tau_C$  is the delay in manual CT.

In the manual case the tracing is effective with probability  $\varepsilon(a_S)$ , with  $a_S$  activity of the index case. The infection and CT transitions are as follows:

$$P + S \xrightarrow{\lambda\delta} P + P \quad A + S \xrightarrow{\lambda\delta\varepsilon} T + P \quad T + S \xrightarrow{\lambda\delta\varepsilon} T + P \quad (1)$$

$$P + S \xrightarrow{\lambda(1-\delta)\varepsilon} P + T \quad A + S \xrightarrow{\lambda(1-\delta)} A + A \quad T + S \xrightarrow{\lambda(1-\delta)} T + A \quad (2)$$

$$P + S \xrightarrow{\lambda(1-\delta)(1-\varepsilon)} P + A \quad A + S \xrightarrow{\lambda\delta(1-\varepsilon)} A + P \quad T + S \xrightarrow{\lambda\delta(1-\varepsilon)} T + P \quad (3)$$

while the spontaneous transitions are:

$$P \xrightarrow{\gamma_P} I \quad A \xrightarrow{\mu} R \quad I \xrightarrow{\mu_I} R \quad (4)$$

$$T \xrightarrow{\gamma_A} Q \quad T \xrightarrow{\mu} R \quad Q \xrightarrow{\mu} R \quad (5)$$

Notice that in the event  $A + S \rightarrow T + P$  both individuals change state; in the event  $T + S \xrightarrow{\lambda\delta\varepsilon} T + P$  the individual  $T$  is traced two times (the second time from the individual she infects while already traced), but this has actually no consequences.

We apply an *activity-attractiveness based mean-field* approach, dividing the population in classes of nodes with same  $(a_S, b_S)$  and considering them statistically equivalent. The model is an exact mean-field since local correlations are continuously destroyed due to link reshuffling: thus the epidemic threshold of the *SIR* and *SIS* epidemic models are the same [2]. Therefore, to obtain the epidemic threshold we consider the mean-field equations for the *SIS* version of the model, in which the recovered nodes become susceptible again without gaining immunity. We assign initially to each node the status of symptomatic (with probability  $\delta$ ) or asymptomatic (with probability  $1 - \delta$ ), instead of assigning it at the time of infection. This choice is completely equivalent to the epidemic model described and allows us to write the mean-field equations in a simpler way. Thus, at the mean-field level, the epidemic dynamics is described by the probabilities:

- $P_{a_S, b_S}(t)$  for a symptomatic node to be infected pre-symptomatic at time  $t$ ;
- $I_{a_S, b_S}(t)$  for a symptomatic node to be infected symptomatic at time  $t$ ;
- $1 - I_{a_S, b_S}(t) - P_{a_S, b_S}(t)$  to be susceptible at time  $t$ , for a node which will develop symptoms;

- $A_{a_S, b_S}(t)$  for an asymptomatic node to be infected asymptomatic at time  $t$ ;
- $T_{a_S, b_S}(t)$  for an asymptomatic node to be infected traced at time  $t$ ;
- $Q_{a_S, b_S}(t)$  for an asymptomatic node to be infected isolated at time  $t$ ;
- $1 - A_{a_S, b_S}(t) - Q_{a_S, b_S}(t) - T_{a_S, b_S}(t)$  to be susceptible at time  $t$ , for a node which will not develop symptoms.

In this case the average attractiveness at time  $t$  is  $\langle b(t) \rangle = \overline{b_S} - (1 - \delta)\overline{b_S Q}(t) - \delta\overline{b_S I}(t)$  where we define in general  $\overline{g} = \int da_S db_S \rho(a_S, b_S) g_{a_S, b_S}$ . We consider the system in the thermodynamic limit. The probabilities previously introduced evolve accordingly to the following equations:

$$\begin{aligned} \partial_t P_{a_S, b_S}(t) = & -\gamma_P P_{a_S, b_S}(t) + \lambda a_S (1 - I_{a_S, b_S}(t) - P_{a_S, b_S}(t)) \frac{\delta\overline{b_S P}(t) + (1 - \delta)[\overline{b_S T}(t) + \overline{b_S A}(t)]}{\overline{b_S} - (1 - \delta)\overline{b_S Q}(t) - \delta\overline{b_S I}(t)} \\ & + \lambda b_S (1 - I_{a_S, b_S}(t) - P_{a_S, b_S}(t)) \frac{\delta\overline{a_S P}(t) + (1 - \delta)[\overline{a_S T}(t) + \overline{a_S A}(t)]}{\overline{b_S} - (1 - \delta)\overline{b_S Q}(t) - \delta\overline{b_S I}(t)} \end{aligned} \quad (6)$$

where the first term on right hand side accounts for symptoms onset; the second and third terms account for contagion processes of a susceptible node who engages a contact with a pre-symptomatic or a non-isolated asymptomatic infected node, respectively for the activation of the susceptible and of the infected node. Both terms are averaged over all the activity-attractiveness classes of the infected node.

$$\partial_t I_{a_S, b_S}(t) = -\mu_I I_{a_S, b_S}(t) + \gamma_P P_{a_S, b_S}(t) \quad (7)$$

where the first term on the right hand side accounts for spontaneous recovery and the second term for spontaneous symptoms development.

$$\begin{aligned} \partial_t A_{a_S, b_S}(t) = & -\mu A_{a_S, b_S}(t) + \lambda a_S (1 - A_{a_S, b_S}(t) - T_{a_S, b_S}(t) - Q_{a_S, b_S}(t)) \frac{\delta[\overline{b_S P}(t) - \varepsilon\overline{b_S P}(t)] + (1 - \delta)[\overline{b_S T}(t) + \overline{b_S A}(t)]}{\overline{b_S} - (1 - \delta)\overline{b_S Q}(t) - \delta\overline{b_S I}(t)} \\ & + \lambda b_S (1 - A_{a_S, b_S}(t) - T_{a_S, b_S}(t) - Q_{a_S, b_S}(t)) \frac{\delta[\overline{a_S P}(t) - \varepsilon\overline{a_S P}(t)] + (1 - \delta)[\overline{a_S T}(t) + \overline{a_S A}(t)]}{\overline{b_S} - (1 - \delta)\overline{b_S Q}(t) - \delta\overline{b_S I}(t)} \\ & - \lambda a_S \delta A_{a_S, b_S}(t) \frac{\overline{\varepsilon b_S} - \varepsilon\overline{b_S I}(t) - \varepsilon\overline{b_S P}(t)}{\overline{b_S} - (1 - \delta)\overline{b_S Q}(t) - \delta\overline{b_S I}(t)} - \lambda b_S \delta A_{a_S, b_S}(t) \frac{\overline{\varepsilon a_S} - \varepsilon\overline{a_S I}(t) - \varepsilon\overline{a_S P}(t)}{\overline{b_S} - (1 - \delta)\overline{b_S Q}(t) - \delta\overline{b_S I}(t)} \end{aligned} \quad (8)$$

where the first term on right hand side accounts for spontaneous recovery; the second and third terms account for contagion processes of a susceptible node who engages a contact with a non-isolated asymptomatic infected node or with a pre-symptomatic node and their contact is not traced ( $(1 - \varepsilon(a'_S))$ , with  $a'_S$  activity of the pre-symptomatic node). Both terms are averaged over all the activity-attractiveness classes of the infected node. The fourth and fifth terms correspond to contact tracing of infected asymptomatic due to infection of a susceptible symptomatic and effective CT of the link ( $\varepsilon(a'_S)$ , with  $a'_S$  activity of the pre-symptomatic node). Both terms are averaged over all the activity-attractiveness classes of the susceptible node.

$$\begin{aligned} \partial_t T_{a_S, b_S}(t) = & -(\mu + \gamma_A) T_{a_S, b_S}(t) + \lambda b_S (1 - A_{a_S, b_S}(t) - T_{a_S, b_S}(t) - Q_{a_S, b_S}(t)) \frac{\delta\overline{a_S P}(t)}{\overline{b_S} - (1 - \delta)\overline{b_S Q}(t) - \delta\overline{b_S I}(t)} \\ & + \lambda a_S (1 - A_{a_S, b_S}(t) - T_{a_S, b_S}(t) - Q_{a_S, b_S}(t)) \frac{\delta\overline{b_S P}(t)}{\overline{b_S} - (1 - \delta)\overline{b_S Q}(t) - \delta\overline{b_S I}(t)} \\ & + \lambda b_S \delta A_{a_S, b_S}(t) \frac{\overline{\varepsilon a_S} - \varepsilon\overline{a_S I}(t) - \varepsilon\overline{a_S P}(t)}{\overline{b_S} - (1 - \delta)\overline{b_S Q}(t) - \delta\overline{b_S I}(t)} \\ & + \lambda a_S \delta A_{a_S, b_S}(t) \frac{\overline{\varepsilon b_S} - \varepsilon\overline{b_S I}(t) - \varepsilon\overline{b_S P}(t)}{\overline{b_S} - (1 - \delta)\overline{b_S Q}(t) - \delta\overline{b_S I}(t)} \end{aligned} \quad (9)$$

where the first term on right hand side accounts for isolation and recovery. The second and third terms account for contagion processes of a susceptible node who engage a contact with a pre-symptomatic node and their contact is traced ( $\varepsilon(a'_S)$ , with  $a'_S$  activity of the pre-symptomatic node). Both terms are averaged over all the activity-attractiveness classes of the infected node. The fourth and fifth terms correspond to contact tracing of infected asymptomatic due to infection of a susceptible symptomatic and effective CT of the link ( $\varepsilon(a'_S)$ , with  $a'_S$  activity of the pre-symptomatic node). Both terms are averaged over all the activity-attractiveness classes of the susceptible node.

$$\partial_t Q_{a_S, b_S}(t) = -\mu Q_{a_S, b_S}(t) + \gamma_A T_{a_S, b_S}(t) \quad (10)$$

where the first term on right hand side accounts for spontaneous recovery and the second term for isolation of traced asymptomatic infected nodes.

This set of equations admits as a stationary state the absorbing state, a configuration where all the population is susceptible. To obtain the condition for the stability of the absorbing state, i.e. the epidemic threshold, we apply a linear stability analysis around the absorbing state.

Let us now consider the case of realistic correlations between the activity and attractiveness [3, 4]:  $\rho(a_S, b_S) = \rho_S(a_S)\delta(b_S - a_S)$ , with generic  $\rho_S(a_S)$ . If we average the equations on all activity classes, we obtain the temporal evolution of the average probabilities  $\overline{P}(t)$ ,  $\overline{I}(t)$ ,  $\overline{A}(t)$ ,  $\overline{T}(t)$ ,  $\overline{Q}(t)$ ; similarly we obtain the temporal evolution of  $\overline{a_S T}(t)$ ,  $\overline{a_S A}(t)$ ,  $\overline{a_S P}(t)$  and  $\overline{\varepsilon a_S P}(t)$  multiplying the equations for  $a_S \rho_S(a_S)$  or  $\varepsilon(a_S) a_S \rho_S(a_S)$  and integrating. Neglecting second order terms in probabilities, we obtain a linearized set of 9 differential equations:

$$\partial_t \overline{I}(t) = -\mu \overline{I}(t) + \gamma_P \overline{P}(t) \quad (11)$$

$$\partial_t \overline{P}(t) = -\gamma_P \overline{P}(t) + 2\lambda[\delta \overline{a_S P}(t) + (1 - \delta)(\overline{a_S T}(t) + \overline{a_S A}(t))] \quad (12)$$

$$\partial_t \overline{Q}(t) = -\mu \overline{Q}(t) + \gamma_A \overline{T}(t) \quad (13)$$

$$\partial_t \overline{T}(t) = -(\mu + \gamma_A) \overline{T}(t) + 2\lambda \delta \overline{\varepsilon a_S P}(t) + 2\lambda \delta \overline{a_S A}(t) \frac{\overline{\varepsilon a_S}}{a_S} \quad (14)$$

$$\partial_t \overline{A}(t) = -\mu \overline{A}(t) + 2\lambda[\delta(\overline{a_S P}(t) - \overline{\varepsilon a_S P}(t)) + (1 - \delta)(\overline{a_S T}(t) + \overline{a_S A}(t))] - 2\lambda \delta \overline{a_S A}(t) \frac{\overline{\varepsilon a_S}}{a_S} \quad (15)$$

$$\partial_t \overline{a_S P}(t) = -\gamma_P \overline{a_S P}(t) + 2\lambda \frac{\overline{a_S^2}}{a_S} [\delta \overline{a_S P}(t) + (1 - \delta)(\overline{a_S T}(t) + \overline{a_S A}(t))] \quad (16)$$

$$\partial_t \overline{\varepsilon a_S P}(t) = -\gamma_P \overline{\varepsilon a_S P}(t) + 2\lambda \frac{\overline{\varepsilon a_S^2}}{a_S} [\delta \overline{a_S P}(t) + (1 - \delta)(\overline{a_S T}(t) + \overline{a_S A}(t))] \quad (17)$$

$$\partial_t \overline{a_S T}(t) = -(\mu + \gamma_A) \overline{a_S T}(t) + 2\lambda \delta \frac{\overline{a_S^2}}{a_S} \overline{\varepsilon a_S P}(t) + 2\lambda \delta \overline{a_S^2 A}(t) \frac{\overline{\varepsilon a_S}}{a_S} \quad (18)$$

$$\partial_t \overline{a_S A}(t) = -\mu \overline{a_S A}(t) + 2\lambda \frac{\overline{a_S^2}}{a_S} [\delta(\overline{a_S P}(t) - \overline{\varepsilon a_S P}(t)) + (1 - \delta)(\overline{a_S T}(t) + \overline{a_S A}(t))] - 2\lambda \delta \overline{a_S^2 A}(t) \frac{\overline{\varepsilon a_S}}{a_S} \quad (19)$$

The linearized equations for the dynamic evolution of  $\overline{a_S^2 A}(t)$  and  $\overline{a_S^2 T}(t)$  always involve terms like  $\overline{a_S^{n+1} A}(t)$ , due to the contact tracing terms. This would produce an infinite set of coupled linear differential equations: to close the equations and obtain a complete set of linearized equations, we express  $\overline{a_S^2 A}(t)$  in terms of the other average probabilities. By definition  $\overline{a_S^2 A}(t) = \int da_S \rho_S(a_S) a_S^2 A_{a_S}(t)$ : since we are interested in studying the absorbing steady state, we consider Eq. (8) for  $\rho(a_S, b_S) = \rho_S(a_S)\delta(b_S - a_S)$ , linearized around the absorbing state and near the stationary condition  $\partial_t A_{a_S}(t) \sim 0$ :

$$A_{a_S}(t) \simeq \frac{2\lambda a_S [\delta(\overline{a_S P}(t) - \overline{\varepsilon a_S P}(t)) + (1 - \delta)(\overline{a_S T}(t) + \overline{a_S A}(t))]}{\mu \overline{a_S} + 2\lambda \delta a_S \overline{\varepsilon a_S}} \quad (20)$$

Thus, setting  $r = \lambda/\mu$  and replacing Eq. (20) into the definition of  $\overline{a_S^2 A}(t)$  we obtain:

$$\overline{a_S^2 A}(t) \simeq \frac{2r}{\overline{a_S}} [\delta(\overline{a_S P}(t) - \overline{\varepsilon a_S P}(t)) + (1 - \delta)(\overline{a_S T}(t) + \overline{a_S A}(t))] K \quad (21)$$

where  $K = \frac{\overline{a_S^3}}{1 + 2r \delta a_S \frac{\overline{\varepsilon a_S}}{\overline{a_S}}} = \int da_S \rho_S(a_S) \frac{a_S^3}{1 + 2r \delta a_S \frac{\overline{\varepsilon a_S}}{\overline{a_S}}}$ .

In this way we obtain the following linearized equations for  $\overline{a_S T}(t)$  and  $\overline{a_S A}(t)$ , near the absorbing stationary state:

$$\partial_t \overline{a_S T}(t) = -(\mu + \gamma_A) \overline{a_S T}(t) + 2\lambda \delta \frac{\overline{a_S^2}}{a_S} \overline{\varepsilon a_S P}(t) + 4\lambda r \frac{\overline{\varepsilon a_S}}{a_S^2} \delta K [\delta(\overline{a_S P}(t) - \overline{\varepsilon a_S P}(t)) + (1 - \delta)(\overline{a_S T}(t) + \overline{a_S A}(t))] \quad (22)$$

$$\begin{aligned} \partial_t \overline{a_S A}(t) = & -\mu \overline{a_S A}(t) + 2\lambda \frac{\overline{a_S^2}}{a_S} [\delta(\overline{a_S P}(t) - \overline{\varepsilon a_S P}(t)) + (1 - \delta)(\overline{a_S T}(t) + \overline{a_S A}(t))] \\ & - 4\lambda r \frac{\overline{\varepsilon a_S}}{a_S^2} \delta K [\delta(\overline{a_S P}(t) - \overline{\varepsilon a_S P}(t)) + (1 - \delta)(\overline{a_S T}(t) + \overline{a_S A}(t))] \end{aligned} \quad (23)$$

We focus on the Jacobian matrix of this set of 9 linearized equations:

$$J = \begin{bmatrix} -\mu_I & \gamma_P & 0 & 0 & 0 & 0 & 0 & 0 & 0 \\ 0 & -\gamma_P & 0 & 0 & 0 & 2\lambda\delta & 0 & 2\lambda(1-\delta) & 2\lambda(1-\delta) \\ 0 & 0 & -\mu & \gamma_A & 0 & 0 & 0 & 0 & 0 \\ 0 & 0 & 0 & -\mu - \gamma_A & 0 & 0 & 2\lambda\delta & 0 & 2\lambda\delta \frac{\varepsilon a_S}{a_S} \\ 0 & 0 & 0 & 0 & -\mu & 2\lambda\delta & -2\lambda\delta & 2\lambda(1-\delta) & 2\lambda(1-\delta) - 2\lambda\delta \frac{\varepsilon a_S}{a_S} \\ 0 & 0 & 0 & 0 & 0 & -\gamma_P + \Delta & 0 & \Gamma & \Gamma \\ 0 & 0 & 0 & 0 & 0 & \phi & -\gamma_P & \Phi & \Phi \\ 0 & 0 & 0 & 0 & 0 & \theta & \Delta - \theta & -\mu - \gamma_A + \Psi & \Psi \\ 0 & 0 & 0 & 0 & 0 & \Delta - \theta & \theta - \Delta & \Gamma - \Psi & -\mu + \Gamma - \Psi \end{bmatrix} = \begin{bmatrix} \mathbb{A}(5 \times 5) & \mathbb{C}(5 \times 4) \\ \mathbb{O}(4 \times 5) & \mathbb{B}(4 \times 4) \end{bmatrix} \quad (24)$$

where  $\Delta = 2\lambda\delta \frac{a_S^2}{a_S}$ ,  $\Gamma = 2\lambda(1-\delta) \frac{a_S^2}{a_S}$ ,  $\phi = 2\lambda\delta \frac{\varepsilon a_S^2}{a_S}$ ,  $\Phi = 2\lambda(1-\delta) \frac{\varepsilon a_S^2}{a_S}$ ,  $\theta = 4\lambda r \delta^2 \frac{\varepsilon a_S}{a_S^2} K$  and  $\Psi = 4\lambda r \delta (1-\delta) \frac{\varepsilon a_S}{a_S^2} K$ .

The Jacobian matrix is a block matrix and the condition for the stability of the absorbing state is obtained imposing all eigenvalues to be negative. We can consider separately the two blocks on the diagonal: for the first block  $\mathbb{A}$  it is evident that the eigenvalues are  $\xi_{1,2} = -\mu$ ,  $\xi_3 = -\mu_I$ ,  $\xi_4 = -\gamma_P$ ,  $\xi_5 = -\mu - \gamma_A$ , all negative. Therefore, it is sufficient to study block  $\mathbb{B}$ , which is a matrix  $4 \times 4$ . The characteristic polynomial of  $\mathbb{B}$  is a polynomial of degree 4, thus we apply the Descartes' rule of signs to impose all roots to be negative and we obtain the condition for the stability of the absorbing state:

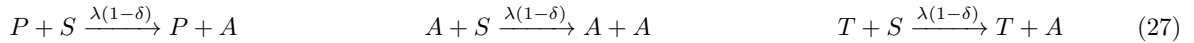
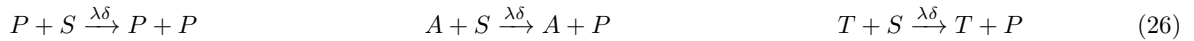
$$8r^3\delta^2(1-\delta) \frac{\varepsilon a_S^2 \varepsilon a_S}{a_S} \frac{a_S^3}{1 + 2r\delta a_S \frac{\varepsilon a_S}{a_S}} \frac{\gamma_A}{\mu} - 4r^2\delta(1-\delta) \left[ \frac{\gamma_A}{\varepsilon a_S^2 a_S^2} + \frac{\gamma_P}{\mu} \frac{a_S^3}{\varepsilon a_S (1 + 2r\delta a_S \frac{\varepsilon a_S}{a_S})} \right] \frac{\gamma_A}{\mu} + 2r a_S^2 a_S \left( \frac{\gamma_A}{\mu} + 1 \right) \left( \delta + \frac{\gamma_P}{\mu} (1-\delta) \right) - a_S^2 \frac{\gamma_P}{\mu} \left( \frac{\gamma_A}{\mu} + 1 \right) < 0 \quad (25)$$

By setting the equality, the equation allows to obtain a closed relation for estimating the epidemic threshold  $\rho_C$ . The epidemic threshold obtained with the mean-field approach is exact and it holds for manual contact tracing, with arbitrary delay  $\tau_C$  (encapsulated in  $\gamma_A$ ), for arbitrary  $\rho_S(a_S)$  and  $\varepsilon(a_S)$ .

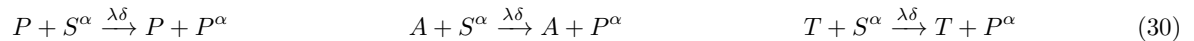
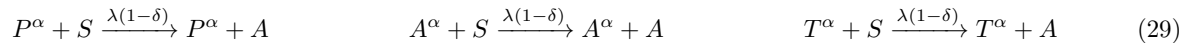
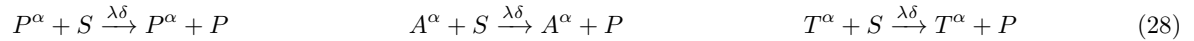
## B. Digital CT

We now focus on the digital CT. Each individual is either endowed or not with the app in the initial condition (with a probability  $f(a_S)$  depending on her activity). This implies that there are different compartments for individuals without the app ( $S, I, P$ , etc.) and with the app (denoted with the superscript  $\alpha$ :  $S^\alpha, I^\alpha, P^\alpha$ , etc.). Notice that, for pure digital CT, necessarily  $T = 0$  and  $Q = 0$ . We nevertheless write here the transitions involving them, that may play a role for hybrid protocols.

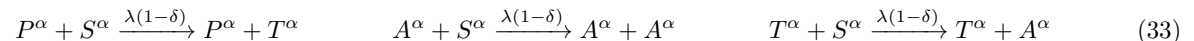
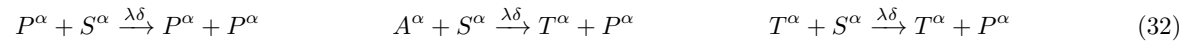
The spontaneous transitions do not depend on whether the individual has the app or not, but the difference with respect to the manual protocol is that  $\tau_C = 0$  so that  $\gamma_A = \gamma_P$ . The infection events are instead as follows. Those involving both individuals without the app (in such a case no new traced individual is generated):



Those involving only one individual with the app (in such a case no new traced individual is generated):



Those involving both individuals with the app (in such a case new traced individuals can be generated):



Analogously to the manual CT we apply the *activity-attractiveness based mean-field* approach to the app-based CT. At the mean-field level, the epidemic dynamics is described by the probabilities:

- $P_{a_S, b_S}(t)$  for a symptomatic node without app to be infected pre-symptomatic at time  $t$ ;
- $I_{a_S, b_S}(t)$  for a symptomatic node without app to be infected symptomatic at time  $t$ ;
- $1 - P_{a_S, b_S}(t) - I_{a_S, b_S}(t)$  to be susceptible at time  $t$ , for a node without app and which will develop symptoms;
- $A_{a_S, b_S}(t)$  for an asymptomatic node without app to be infected asymptomatic at time  $t$ ;
- $1 - A_{a_S, b_S}(t)$  to be susceptible at time  $t$ , for a node without app and which will not develop symptoms;
- $P_{a_S, b_S}^\alpha(t)$  for a symptomatic node with app to be infected pre-symptomatic at time  $t$ ;
- $I_{a_S, b_S}^\alpha(t)$  for a symptomatic node with app to be infected symptomatic at time  $t$ ;
- $1 - P_{a_S, b_S}^\alpha(t) - I_{a_S, b_S}^\alpha(t)$  to be susceptible at time  $t$ , for a node with app and which will develop symptoms;
- $A_{a_S, b_S}^\alpha(t)$  for an asymptomatic node with app to be infected asymptomatic at time  $t$ ;
- $T_{a_S, b_S}^\alpha(t)$  for an asymptomatic node with app to be infected traced at time  $t$ ;
- $Q_{a_S, b_S}^\alpha(t)$  for an asymptomatic node with app to be infected isolated at time  $t$ ;
- $1 - A_{a_S, b_S}^\alpha(t) - Q_{a_S, b_S}^\alpha(t) - T_{a_S, b_S}^\alpha(t)$  to be susceptible at time  $t$ , for a node with app and which will not develop symptoms.

In this case the average attractiveness at time  $t$  is  $\langle b(t) \rangle = \overline{b_S} - (1 - \delta)\overline{fb_S Q^\alpha(t)} - \delta(\overline{fb_S I^\alpha(t)} + \overline{(1 - f)b_S I(t)})$ . We consider the system in the thermodynamic limit: the probabilities previously introduced evolve according to the following equations, obtained analogously to those for manual CT:

$$\partial_t I_{a_S, b_S}(t) = -\mu_I I_{a_S, b_S}(t) + \gamma_P P_{a_S, b_S}(t) \quad (34)$$

$$\begin{aligned} \partial_t P_{a_S, b_S}(t) = & -\gamma_P P_{a_S, b_S}(t) \\ & + \lambda a_S (1 - I_{a_S, b_S}(t) - P_{a_S, b_S}(t)) \frac{\delta(\overline{fb_S P^\alpha(t)} + \overline{(1 - f)b_S P(t)} + (1 - \delta)\overline{fb_S T^\alpha(t)} + \overline{fb_S A^\alpha(t)} + \overline{(1 - f)b_S A(t)})}{\overline{b_S} - (1 - \delta)\overline{fb_S Q^\alpha(t)} - \delta(\overline{fb_S I^\alpha(t)} + \overline{(1 - f)b_S I(t)})} \\ & + \lambda b_S (1 - I_{a_S, b_S}(t) - P_{a_S, b_S}(t)) \frac{\delta(\overline{f a_S P^\alpha(t)} + \overline{(1 - f)a_S P(t)} + (1 - \delta)\overline{f a_S T^\alpha(t)} + \overline{f a_S A^\alpha(t)} + \overline{(1 - f)a_S A(t)})}{\overline{b_S} - (1 - \delta)\overline{fb_S Q^\alpha(t)} - \delta(\overline{fb_S I^\alpha(t)} + \overline{(1 - f)b_S I(t)})} \end{aligned} \quad (35)$$

$$\partial_t I_{a_S, b_S}^\alpha(t) = -\mu_I I_{a_S, b_S}^\alpha(t) + \gamma_P P_{a_S, b_S}^\alpha(t) \quad (36)$$

$$\begin{aligned} \partial_t P_{a_S, b_S}^\alpha(t) = & -\gamma_P P_{a_S, b_S}^\alpha(t) \\ & + \lambda a_S (1 - I_{a_S, b_S}^\alpha(t) - P_{a_S, b_S}^\alpha(t)) \frac{\delta(\overline{fb_S P^\alpha(t)} + \overline{(1 - f)b_S P(t)} + (1 - \delta)\overline{fb_S T^\alpha(t)} + \overline{fb_S A^\alpha(t)} + \overline{(1 - f)b_S A(t)})}{\overline{b_S} - (1 - \delta)\overline{fb_S Q^\alpha(t)} - \delta(\overline{fb_S I^\alpha(t)} + \overline{(1 - f)b_S I(t)})} \\ & + \lambda b_S (1 - I_{a_S, b_S}^\alpha(t) - P_{a_S, b_S}^\alpha(t)) \frac{\delta(\overline{f a_S P^\alpha(t)} + \overline{(1 - f)a_S P(t)} + (1 - \delta)\overline{f a_S T^\alpha(t)} + \overline{f a_S A^\alpha(t)} + \overline{(1 - f)a_S A(t)})}{\overline{b_S} - (1 - \delta)\overline{fb_S Q^\alpha(t)} - \delta(\overline{fb_S I^\alpha(t)} + \overline{(1 - f)b_S I(t)})} \end{aligned} \quad (37)$$

$$\begin{aligned} \partial_t A_{a_S, b_S}(t) = & -\mu A_{a_S, b_S}(t) \\ & + \lambda a_S (1 - A_{a_S, b_S}(t)) \frac{\delta(\overline{fb_S P^\alpha(t)} + \overline{(1 - f)b_S P(t)} + (1 - \delta)\overline{fb_S T^\alpha(t)} + \overline{fb_S A^\alpha(t)} + \overline{(1 - f)b_S A(t)})}{\overline{b_S} - (1 - \delta)\overline{fb_S Q^\alpha(t)} - \delta(\overline{fb_S I^\alpha(t)} + \overline{(1 - f)b_S I(t)})} \\ & + \lambda b_S (1 - A_{a_S, b_S}(t)) \frac{\delta(\overline{f a_S P^\alpha(t)} + \overline{(1 - f)a_S P(t)} + (1 - \delta)\overline{f a_S T^\alpha(t)} + \overline{f a_S A^\alpha(t)} + \overline{(1 - f)a_S A(t)})}{\overline{b_S} - (1 - \delta)\overline{fb_S Q^\alpha(t)} - \delta(\overline{fb_S I^\alpha(t)} + \overline{(1 - f)b_S I(t)})} \end{aligned} \quad (38)$$

$$\begin{aligned} \partial_t A_{a_S, b_S}^\alpha(t) = & -\mu A_{a_S, b_S}^\alpha(t) \\ & + \lambda a_S (1 - A_{a_S, b_S}^\alpha(t) - T_{a_S, b_S}^\alpha(t) - Q_{a_S, b_S}^\alpha(t)) \frac{\delta(\overline{(1 - f)b_S P(t)} + (1 - \delta)\overline{fb_S T^\alpha(t)} + \overline{fb_S A^\alpha(t)} + \overline{(1 - f)b_S A(t)})}{\overline{b_S} - (1 - \delta)\overline{fb_S Q^\alpha(t)} - \delta(\overline{fb_S I^\alpha(t)} + \overline{(1 - f)b_S I(t)})} \\ & + \lambda b_S (1 - A_{a_S, b_S}^\alpha(t) - T_{a_S, b_S}^\alpha(t) - Q_{a_S, b_S}^\alpha(t)) \frac{\delta(\overline{(1 - f)a_S P(t)} + (1 - \delta)\overline{f a_S T^\alpha(t)} + \overline{f a_S A^\alpha(t)} + \overline{(1 - f)a_S A(t)})}{\overline{b_S} - (1 - \delta)\overline{fb_S Q^\alpha(t)} - \delta(\overline{fb_S I^\alpha(t)} + \overline{(1 - f)b_S I(t)})} \\ & - \lambda \delta a_S A_{a_S, b_S}^\alpha(t) \frac{\overline{fb_S} - \overline{fb_S P^\alpha(t)} - \overline{fb_S I^\alpha(t)}}{\overline{b_S} - (1 - \delta)\overline{fb_S Q^\alpha(t)} - \delta(\overline{fb_S I^\alpha(t)} + \overline{(1 - f)b_S I(t)})} \\ & - \lambda \delta b_S A_{a_S, b_S}^\alpha(t) \frac{\overline{f a_S} - \overline{f a_S P^\alpha(t)} - \overline{f a_S I^\alpha(t)}}{\overline{b_S} - (1 - \delta)\overline{fb_S Q^\alpha(t)} - \delta(\overline{fb_S I^\alpha(t)} + \overline{(1 - f)b_S I(t)})} \end{aligned} \quad (39)$$

$$\partial_t Q_{a_S, b_S}^\alpha(t) = -\mu Q_{a_S, b_S}^\alpha(t) + \gamma_P T_{a_S, b_S}^\alpha(t) \quad (40)$$

$$\partial_t T_{a_S, b_S}^\alpha(t) = -(\mu + \gamma_P) T_{a_S, b_S}^\alpha(t) \quad (41)$$

$$\begin{aligned} & + \lambda a_S (1 - A_{a_S, b_S}^\alpha(t) - T_{a_S, b_S}^\alpha(t) - Q_{a_S, b_S}^\alpha(t)) \frac{\overline{\delta f b_S P^\alpha(t)}}{\overline{b_S - (1 - \delta) f b_S Q^\alpha(t) - \delta (f b_S I^\alpha(t) + (1 - f) b_S I(t)}}} \\ & + \lambda b_S (1 - A_{a_S, b_S}^\alpha(t) - T_{a_S, b_S}^\alpha(t) - Q_{a_S, b_S}^\alpha(t)) \frac{\overline{\delta f a_S P^\alpha(t)}}{\overline{b_S - (1 - \delta) f b_S Q^\alpha(t) - \delta (f b_S I^\alpha(t) + (1 - f) b_S I(t)}}} \\ & + \lambda \delta a_S A_{a_S, b_S}^\alpha(t) \frac{\overline{f b_S - f b_S P^\alpha(t) - f b_S I^\alpha(t)}}{\overline{b_S - (1 - \delta) f b_S Q^\alpha(t) - \delta (f b_S I^\alpha(t) + (1 - f) b_S I(t)}}} \\ & + \lambda \delta b_S A_{a_S, b_S}^\alpha(t) \frac{\overline{f a_S - f a_S P^\alpha(t) - f a_S I^\alpha(t)}}{\overline{b_S - (1 - \delta) f b_S Q^\alpha(t) - \delta (f b_S I^\alpha(t) + (1 - f) b_S I(t)}}} \end{aligned}$$

This set of equations admits as a stationary state the absorbing state, a configuration where all the population is susceptible. To obtain the condition for the stability of the absorbing state, i.e. the epidemic threshold, we apply a linear stability analysis around the absorbing state.

Let us now consider the case of realistic correlations between the activity and attractiveness:  $\rho(a_S, b_S) = \rho_S(a_S) \delta(b_S - a_S)$ , with general  $\rho_S(a_S)$ . If we average on all activity classes, we obtain the temporal evolution of the average probabilities  $\overline{P(t)}$ ,  $\overline{I(t)}$ ,  $\overline{A(t)}$ ,  $\overline{P^\alpha(t)}$ ,  $\overline{I^\alpha(t)}$ ,  $\overline{A^\alpha(t)}$ ,  $\overline{Q^\alpha(t)}$ ,  $\overline{T^\alpha(t)}$ ; similarly we obtain the temporal evolution of  $\overline{f a_S P^\alpha(t)}$ ,  $\overline{f a_S T^\alpha(t)}$ ,  $\overline{a_S A^\alpha(t)}$ ,  $\overline{f a_S A^\alpha(t)}$ ,  $\overline{(1 - f) a_S P(t)}$ ,  $\overline{(1 - f) a_S A(t)}$ , multiplying the equations for  $f(a_S) a_S \rho_S(a_S)$  or  $a_S \rho_S(a_S)$  or  $(1 - f(a_S)) a_S \rho_S(a_S)$  and integrating over all activity classes. We neglect the terms of second order in probabilities obtaining a linearized set of 14 differential equations:

$$\partial_t \overline{I(t)} = -\mu \overline{I(t)} + \gamma_P \overline{P(t)} \quad (42)$$

$$\partial_t \overline{P(t)} = -\gamma_P \overline{P(t)} + 2\lambda [\delta (\overline{f a_S P^\alpha(t)} + \overline{(1 - f) a_S P(t)}) + (1 - \delta) (\overline{f a_S T^\alpha(t)} + \overline{f a_S A^\alpha(t)} + \overline{(1 - f) a_S A(t)})] \quad (43)$$

$$\partial_t \overline{I^\alpha(t)} = -\mu \overline{I^\alpha(t)} + \gamma_P \overline{P^\alpha(t)} \quad (44)$$

$$\partial_t \overline{P^\alpha(t)} = -\gamma_P \overline{P^\alpha(t)} + 2\lambda [\delta (\overline{f a_S P^\alpha(t)} + \overline{(1 - f) a_S P(t)}) + (1 - \delta) (\overline{f a_S T^\alpha(t)} + \overline{f a_S A^\alpha(t)} + \overline{(1 - f) a_S A(t)})] \quad (45)$$

$$\partial_t \overline{A(t)} = -\mu \overline{A(t)} + 2\lambda [\delta (\overline{f a_S P^\alpha(t)} + \overline{(1 - f) a_S P(t)}) + (1 - \delta) (\overline{f a_S T^\alpha(t)} + \overline{f a_S A^\alpha(t)} + \overline{(1 - f) a_S A(t)})] \quad (46)$$

$$\partial_t \overline{Q^\alpha(t)} = -\mu \overline{Q^\alpha(t)} + \gamma_P \overline{T^\alpha(t)} \quad (47)$$

$$\partial_t \overline{T^\alpha(t)} = -(\mu + \gamma_P) \overline{T^\alpha(t)} + 2\lambda \delta \overline{f a_S P^\alpha(t)} + 2\lambda \delta \overline{a_S A^\alpha(t)} \frac{\overline{f a_S}}{\overline{a_S}} \quad (48)$$

$$\partial_t \overline{A^\alpha(t)} = -\mu \overline{A^\alpha(t)} + 2\lambda [\delta (\overline{(1 - f) a_S P(t)} + (1 - \delta) (\overline{f a_S T^\alpha(t)} + \overline{f a_S A^\alpha(t)} + \overline{(1 - f) a_S A(t)})] \quad (49)$$

$$- 2\lambda \delta \overline{a_S A^\alpha(t)} \frac{\overline{f a_S}}{\overline{a_S}}$$

$$\partial_t \overline{a_S A^\alpha(t)} = -\mu \overline{a_S A^\alpha(t)} + 2\lambda \frac{\overline{a_S^2}}{\overline{a_S}} [\delta (\overline{(1 - f) a_S P(t)} + (1 - \delta) (\overline{f a_S T^\alpha(t)} + \overline{f a_S A^\alpha(t)} + \overline{(1 - f) a_S A(t)})] \quad (50)$$

$$- 2\lambda \delta \overline{a_S^2 A^\alpha(t)} \frac{\overline{f a_S}}{\overline{a_S}}$$

$$\partial_t \overline{f a_S P^\alpha(t)} = -\gamma_P \overline{f a_S P^\alpha(t)} \quad (51)$$

$$+ 2\lambda \frac{\overline{f a_S^2}}{\overline{a_S}} [\delta (\overline{f a_S P^\alpha(t)} + \overline{(1 - f) a_S P(t)}) + (1 - \delta) (\overline{f a_S T^\alpha(t)} + \overline{f a_S A^\alpha(t)} + \overline{(1 - f) a_S A(t)})]$$

$$\partial_t \overline{(1 - f) a_S P(t)} = -\gamma_P \overline{(1 - f) a_S P(t)}$$

$$+ 2\lambda \frac{\overline{(1 - f) a_S^2}}{\overline{a_S}} [\delta (\overline{f a_S P^\alpha(t)} + \overline{(1 - f) a_S P(t)}) + (1 - \delta) (\overline{f a_S T^\alpha(t)} + \overline{f a_S A^\alpha(t)} + \overline{(1 - f) a_S A(t)})] \quad (52)$$

$$\partial_t \overline{(1 - f) a_S A(t)} = -\mu \overline{(1 - f) a_S A(t)}$$

$$+ 2\lambda \frac{\overline{(1 - f) a_S^2}}{\overline{a_S}} [\delta (\overline{f a_S P^\alpha(t)} + \overline{(1 - f) a_S P(t)}) + (1 - \delta) (\overline{f a_S T^\alpha(t)} + \overline{f a_S A^\alpha(t)} + \overline{(1 - f) a_S A(t)})] \quad (53)$$

$$\partial_t \overline{f a_S T^\alpha(t)} = -(\mu + \gamma_P) \overline{f a_S T^\alpha(t)} + 2\lambda \delta \frac{\overline{f a_S^2}}{\overline{a_S}} \overline{f a_S P^\alpha(t)} + 2\lambda \delta \overline{f a_S^2 A^\alpha(t)} \frac{\overline{f a_S}}{\overline{a_S}} \quad (54)$$

$$\partial_t \overline{f a_S A^\alpha(t)} = -\mu \overline{f a_S A^\alpha(t)} + 2\lambda \frac{\overline{f a_S^2}}{\overline{a_S}} [\delta (\overline{(1 - f) a_S P(t)} + (1 - \delta) (\overline{f a_S T^\alpha(t)} + \overline{f a_S A^\alpha(t)} + \overline{(1 - f) a_S A(t)})] \quad (55)$$

$$- 2\lambda \delta \overline{f a_S^2 A^\alpha(t)} \frac{\overline{f a_S}}{\overline{a_S}}$$

Similarly to the manual CT, in order to close the equations and obtain a complete set of linearized equations, we express  $\overline{f a_S^2 A^\alpha(t)}$  and  $\overline{a_S^2 A^\alpha(t)}$  in terms of the other average probabilities using their own definition. By

definition  $\overline{fa_S^2 A^\alpha}(t) = \int da_S \rho_S(a_S) f(a_S) a_S^2 A_{a_S}^\alpha(t)$  and  $\overline{a_S^2 A^\alpha}(t) = \int da_S \rho_S(a_S) a_S^2 A_{a_S}^\alpha(t)$ : since we are interested in studying the steady state and its stability, we consider the Eq. (39) for  $\rho(a_S, b_S) = \rho_S(a_S) \delta(b_S - a_S)$ , linearized around the absorbing state and near to the stationary condition  $\partial_t A_{a_S}^\alpha(t) \sim 0$ :

$$A_{a_S}^\alpha(t) \simeq \frac{2\lambda a_S [\delta \overline{(1-f)a_S P}(t) + (1-\delta)(\overline{fa_S T^\alpha}(t) + \overline{fa_S A^\alpha}(t) + \overline{(1-f)a_S A}(t))]}{\mu \overline{a_S} + 2\lambda \delta a_S \overline{fa_S}} \quad (56)$$

Thus,

$$\overline{fa_S^2 A^\alpha}(t) \simeq \frac{2}{\overline{a_S}} r [\delta \overline{(1-f)a_S P}(t) + (1-\delta)(\overline{fa_S T^\alpha}(t) + \overline{fa_S A^\alpha}(t) + \overline{(1-f)a_S A}(t))] H \quad (57)$$

$$\overline{a_S^2 A^\alpha}(t) \simeq \frac{2}{\overline{a_S}} r [\delta \overline{(1-f)a_S P}(t) + (1-\delta)(\overline{fa_S T^\alpha}(t) + \overline{fa_S A^\alpha}(t) + \overline{(1-f)a_S A}(t))] Z \quad (58)$$

$$\text{where } H = \frac{\overline{fa_S^3}}{1+2r\delta a_S \frac{\overline{fa_S}}{\overline{a_S}}} = \int da_S \rho_S(a_S) \frac{f(a_S) a_S^3}{1+2r\delta a_S \frac{\overline{fa_S}}{\overline{a_S}}}, \quad Z = \frac{\overline{a_S^3}}{1+2r\delta a_S \frac{\overline{fa_S}}{\overline{a_S}}}.$$

In this way we obtain the following linearized equations for  $\overline{fa_S T^\alpha}$ ,  $\overline{fa_S A^\alpha}$  and  $\overline{a_S A^\alpha}$  near the absorbing stationary state:

$$\begin{aligned} \partial_t \overline{a_S A^\alpha}(t) &= -\mu \overline{a_S A^\alpha}(t) + 2\lambda \frac{\overline{a_S^2}}{\overline{a_S}} [\delta \overline{(1-f)a_S P}(t) + (1-\delta)(\overline{fa_S T^\alpha}(t) + \overline{fa_S A^\alpha}(t) + \overline{(1-f)a_S A}(t))] \\ &\quad - 4\lambda r \delta \frac{\overline{fa_S}}{\overline{a_S^2}} [\delta \overline{(1-f)a_S P}(t) + (1-\delta)(\overline{fa_S T^\alpha}(t) + \overline{fa_S A^\alpha}(t) + \overline{(1-f)a_S A}(t))] Z \end{aligned} \quad (59)$$

$$\begin{aligned} \partial_t \overline{fa_S T^\alpha}(t) &= -(\mu + \gamma_P) \overline{fa_S T^\alpha}(t) + 2\lambda \delta \frac{\overline{fa_S^2}}{\overline{a_S}} \overline{fa_S P^\alpha}(t) \\ &\quad + 4\lambda r \delta \frac{\overline{fa_S}}{\overline{a_S^2}} [\delta \overline{(1-f)a_S P}(t) + (1-\delta)(\overline{fa_S T^\alpha}(t) + \overline{fa_S A^\alpha}(t) + \overline{(1-f)a_S A}(t))] H \end{aligned} \quad (60)$$

$$\begin{aligned} \partial_t \overline{fa_S A^\alpha}(t) &= -\mu \overline{fa_S A^\alpha}(t) + 2\lambda \frac{\overline{fa_S^2}}{\overline{a_S}} [\delta \overline{(1-f)a_S P}(t) + (1-\delta)(\overline{fa_S T^\alpha}(t) + \overline{fa_S A^\alpha}(t) + \overline{(1-f)a_S A}(t))] \\ &\quad - 4\lambda r \delta \frac{\overline{fa_S}}{\overline{a_S^2}} [\delta \overline{(1-f)a_S P}(t) + (1-\delta)(\overline{fa_S T^\alpha}(t) + \overline{fa_S A^\alpha}(t) + \overline{(1-f)a_S A}(t))] H \end{aligned} \quad (61)$$

Focusing on the Jacobian matrix of this set of 14 linearized equations:

$$\begin{aligned} J &= \begin{bmatrix} -\mu_I & \gamma_P & 0 & 0 & 0 & 0 & 0 & 0 & 0 & 0 & 0 & 0 & 0 & 0 \\ 0 & -\gamma_P & 0 & 0 & 0 & 0 & 0 & 0 & 0 & 2\lambda\delta & 2\lambda\delta & 2\lambda(1-\delta) & 2\lambda(1-\delta) & 2\lambda(1-\delta) \\ 0 & 0 & -\mu_I & \gamma_P & 0 & 0 & 0 & 0 & 0 & 0 & 0 & 0 & 0 & 0 \\ 0 & 0 & 0 & -\gamma_P & 0 & 0 & 0 & 0 & 0 & 2\lambda\delta & 2\lambda\delta & 2\lambda(1-\delta) & 2\lambda(1-\delta) & 2\lambda(1-\delta) \\ 0 & 0 & 0 & 0 & -\mu & 0 & 0 & 0 & 0 & 2\lambda\delta & 2\lambda\delta & 2\lambda(1-\delta) & 2\lambda(1-\delta) & 2\lambda(1-\delta) \\ 0 & 0 & 0 & 0 & 0 & -\mu & +\gamma_P & 0 & 0 & 0 & 0 & 0 & 0 & 0 \\ 0 & 0 & 0 & 0 & 0 & 0 & -\mu - \gamma_P & 0 & 2\lambda\delta \frac{\overline{fa_S}}{\overline{a_S}} & 2\lambda\delta & 0 & 0 & 0 & 0 \\ 0 & 0 & 0 & 0 & 0 & 0 & 0 & -\mu & -2\lambda\delta \frac{\overline{fa_S}}{\overline{a_S}} & 0 & 2\lambda\delta & 2\lambda(1-\delta) & 2\lambda(1-\delta) & 2\lambda(1-\delta) \\ 0 & 0 & 0 & 0 & 0 & 0 & 0 & 0 & -\mu & 0 & \Delta + \phi - \Phi \frac{Z}{H} & \theta + \Gamma - \Psi \frac{Z}{H} & \theta + \Gamma - \Psi \frac{Z}{H} & \theta + \Gamma - \Psi \frac{Z}{H} \\ 0 & 0 & 0 & 0 & 0 & 0 & 0 & 0 & 0 & -\gamma_P + \Delta & \Delta & \Gamma & \Gamma & \Gamma \\ 0 & 0 & 0 & 0 & 0 & 0 & 0 & 0 & 0 & \phi & -\gamma_P + \phi & \theta & \theta & \theta \\ 0 & 0 & 0 & 0 & 0 & 0 & 0 & 0 & 0 & \phi & \phi & -\mu + \theta & \theta & \theta \\ 0 & 0 & 0 & 0 & 0 & 0 & 0 & 0 & 0 & \Delta & \Phi & \Psi & -\mu - \gamma_P + \Psi & \Psi \\ 0 & 0 & 0 & 0 & 0 & 0 & 0 & 0 & 0 & 0 & \Delta - \Phi & \Gamma - \Psi & \Gamma - \Psi & -\mu + \Gamma - \Psi \end{bmatrix} \\ &= \begin{bmatrix} \mathbb{A}(9 \times 9) & \mathbb{C}(9 \times 5) \\ \mathbb{O}(5 \times 9) & \mathbb{B}(5 \times 5) \end{bmatrix} \end{aligned} \quad (62)$$

where  $\Delta = 2\lambda\delta \frac{\overline{fa_S^2}}{\overline{a_S}}$ ,  $\Gamma = 2\lambda(1-\delta) \frac{\overline{fa_S^2}}{\overline{a_S}}$ ,  $\phi = 2\lambda\delta \frac{\overline{(1-f)a_S^2}}{\overline{a_S}}$ ,  $\theta = 2\lambda(1-\delta) \frac{\overline{(1-f)a_S^2}}{\overline{a_S}}$ ,  $\Phi = 4\lambda r \delta^2 \frac{\overline{fa_S}}{\overline{a_S^2}} H$  and  $\Psi = 4\lambda r \delta (1-\delta) \frac{\overline{fa_S}}{\overline{a_S^2}} H$ .

The Jacobian matrix is a block matrix and we can consider separately the two blocks on the diagonal: for the first block  $\mathbb{A}$  it is evident that the eigenvalues are  $\xi_{1,2} = -\mu_I$ ,  $\xi_{3,4,5,6} = -\mu$ ,  $\xi_{7,8} = -\gamma_P$ ,  $\xi_9 = -\mu - \gamma_P$ , all negative. Therefore, it is sufficient to study block  $\mathbb{B}$ , which is a matrix  $5 \times 5$ . The characteristic polynomial of

$\mathbb{B}$  is a polynomial of degree 5: we apply the Descartes' rule of signs, to impose all roots to be negative and we obtain the condition for the stability of the absorbing state:

$$8r^3\delta^2(1-\delta)\frac{\overline{fa_S^2 f a_S}}{\overline{a_S}}\frac{\overline{fa_S^3}}{1+2r\delta a_S\frac{\overline{fa_S}}{\overline{a_S}}}\frac{\gamma_P}{\mu} - 4r^2\delta(1-\delta)\left[\frac{\overline{fa_S^2}}{\mu} + \frac{\gamma_P}{\mu}\frac{\overline{fa_S^3}}{1+2r\delta a_S\frac{\overline{fa_S}}{\overline{a_S}}}\right]\frac{\gamma_P}{\mu} \quad (63)$$

$$+ 2r\overline{a_S^2 a_S}\left(\frac{\gamma_P}{\mu} + 1\right)\left(\delta + \frac{\gamma_P}{\mu}(1-\delta)\right) - \overline{a_S^2}\frac{\gamma_P}{\mu}\left(\frac{\gamma_P}{\mu} + 1\right) < 0$$

By setting the equality, the equation allows to obtain a closed relation for an estimate of the epidemic threshold. The epidemic threshold obtained with the mean-field approach is exact and it holds for digital contact tracing, with arbitrary  $\rho_S(a_S)$  and  $f(a_S)$ .

### C. Hybrid CT

We now focus on the hybrid CT, with simultaneous implementation of both digital and manual CT. The transitions occurring in this case can be deduced starting from the transitions described above for manual and digital CT. A relevant difference is the need to consider an additional compartment,  $T_M^\alpha$ , indicating individual endowed with the app that are nevertheless traced manually, so that their transition to the  $Q^\alpha$  state occurs with a rate  $\gamma_A$ . In a manner analogous to the previous cases, we apply the *activity-attractiveness based mean-field* approach to the hybrid CT. At the mean-field level, the epidemic dynamics is described by the probabilities defined for the digital CT, with these additional/redefined probabilities:

- $T_{a_S, b_S|M}^\alpha(t)$  for an asymptomatic node with app to be infected and traced manually;
- $T_{a_S, b_S}(t)$  for an asymptomatic node without the app to be infected and traced manually;
- $Q_{a_S, b_S}(t)$  for an asymptomatic node without the app to be isolated;
- $1 - A_{a_S, b_S}(t) - Q_{a_S, b_S}(t) - T_{a_S, b_S}(t)$  to be susceptible at time  $t$ , for a node without app and which will not develop symptoms;
- $1 - A_{a_S, b_S}^\alpha(t) - Q_{a_S, b_S}^\alpha(t) - T_{a_S, b_S}^\alpha(t) - T_{a_S, b_S|M}^\alpha(t)$  to be susceptible at time  $t$ , for a node with app and which will not develop symptoms;

We consider the system in the thermodynamic limit and for  $\rho(a_S, b_S) = \rho_S(a_S)\delta(b_S - a_S)$ : in this case the average attractiveness at time  $t$  is  $\langle b(t) \rangle = \overline{a_S} - (1-\delta)(\overline{fa_S Q^\alpha(t)} + (1-f)a_S Q(t)) - \delta(\overline{fa_S I^\alpha(t)} + (1-f)a_S I(t))$ . The probabilities introduced evolve according to the following equations, obtained analogously to those for manual and digital CT:

$$\partial_t P_{a_S}(t) = -\gamma_P P_{a_S}(t) + 2\lambda(1 - P_{a_S}(t) - I_{a_S}(t))\frac{a_S}{\langle b(t) \rangle} [\delta(\overline{a_S f P^\alpha(t)} + \overline{a_S(1-f)P(t)}) \quad (64)$$

$$+ (1-\delta)(\overline{a_S f A^\alpha(t)} + \overline{a_S f T^\alpha(t)} + \overline{a_S f T_M^\alpha(t)} + \overline{a_S(1-f)T(t)} + \overline{a_S(1-f)A(t)})]$$

$$\partial_t I_{a_S}(t) = -\mu_I I_{a_S}(t) + \gamma_P P_{a_S}(t) \quad (65)$$

$$\partial_t P_{a_S}^\alpha(t) = -\gamma_P P_{a_S}^\alpha(t) + 2\lambda(1 - P_{a_S}^\alpha(t) - I_{a_S}^\alpha(t))\frac{a_S}{\langle b(t) \rangle} [\delta(\overline{a_S f P^\alpha(t)} + \overline{a_S(1-f)P(t)}) \quad (66)$$

$$+ (1-\delta)(\overline{a_S f A^\alpha(t)} + \overline{a_S f T^\alpha(t)} + \overline{a_S f T_M^\alpha(t)} + \overline{a_S(1-f)T(t)} + \overline{a_S(1-f)A(t)})]$$

$$\partial_t I_{a_S}^\alpha(t) = -\mu_I I_{a_S}^\alpha(t) + \gamma_P P_{a_S}^\alpha(t) \quad (67)$$

$$\partial_t A_{a_S}(t) = -\mu A_{a_S}(t) + 2\lambda(1 - A_{a_S}(t) - T_{a_S}(t) - Q_{a_S}(t))\frac{a_S}{\langle b(t) \rangle} [\delta(\overline{a_S(1-\varepsilon)fP^\alpha(t)} + \overline{a_S(1-\varepsilon)(1-f)P(t)}) \quad (68)$$

$$+ (1-\delta)(\overline{a_S f A^\alpha(t)} + \overline{a_S f T^\alpha(t)} + \overline{a_S f T_M^\alpha(t)} + \overline{a_S(1-f)T(t)} + \overline{a_S(1-f)A(t)})]$$

$$- 2\lambda\delta A_{a_S}(t)\frac{a_S}{\langle b(t) \rangle} [(\overline{a_S \varepsilon f} - \overline{a_S \varepsilon f P^\alpha(t)} - \overline{a_S \varepsilon f I^\alpha(t)}) + (\overline{a_S \varepsilon(1-f)} - \overline{a_S \varepsilon(1-f)P(t)} - \overline{a_S \varepsilon(1-f)I(t)})]$$

$$\partial_t T_{a_S}(t) = -(\mu + \gamma_A)T_{a_S}(t) + 2\lambda\delta\frac{a_S}{\langle b(t) \rangle} (1 - A_{a_S}(t) - T_{a_S}(t) - Q_{a_S}(t))[\overline{a_S \varepsilon f P^\alpha(t)} + \overline{a_S \varepsilon(1-f)P(t)}]$$

$$+ 2\lambda\delta A_{a_S}(t)\frac{a_S}{\langle b(t) \rangle} [(\overline{a_S \varepsilon f} - \overline{a_S \varepsilon f P^\alpha(t)} - \overline{a_S \varepsilon f I^\alpha(t)}) + (\overline{a_S \varepsilon(1-f)} - \overline{a_S \varepsilon(1-f)P(t)} - \overline{a_S \varepsilon(1-f)I(t)})]$$

$$(69)$$

$$\partial_t Q_{a_S}(t) = -\mu Q_{a_S}(t) + \gamma_A T_{a_S}(t) \quad (70)$$



with  $\Psi = 2\lambda \frac{a_S^2}{a_S} - 4\lambda r \delta \frac{a_S \varepsilon}{a_S^2} K$ ,  $\theta = 2\lambda \frac{a_S^2}{a_S} - 4\lambda r \delta \frac{a_S \varepsilon (1-f) + a_S f}{a_S^2} J$ ,  $K = \frac{a_S^3}{1+2ra_S \delta \frac{a_S \varepsilon}{a_S}}$  and  $J = \frac{a_S^3}{1+2ra_S \delta \frac{a_S f + a_S \varepsilon (1-f)}{a_S}}$ .

$$\mathbb{B} = \begin{bmatrix} -\gamma_P & 0 & \Xi \delta & \Xi \delta & \Xi \sigma \\ 0 & -\gamma_P & \Pi \delta & \Pi \delta & \Pi \sigma \\ 0 & 0 & -\gamma_P + \Delta \delta & \Delta \delta & \Delta \sigma \\ 0 & 0 & \beta \delta & -\gamma_P + \beta \delta & \beta \sigma \\ \Omega \delta & \Omega \delta & \phi \delta & \phi \delta & -\mu - \gamma_A + \phi \sigma & \phi \sigma & \phi \sigma & \phi \sigma & \phi \sigma \\ -\Gamma \delta & 0 & \Gamma \delta & \beta \delta & \Gamma \sigma & -\mu - \gamma_P + \Gamma \sigma & \Gamma \sigma & \Gamma \sigma & \Gamma \sigma \\ \Sigma \delta & 0 & \Phi \delta & 0 & \Phi \sigma & \Phi \sigma & -\mu - \gamma_A + \Phi \sigma & \Phi \sigma & \Phi \sigma \\ -\Omega \delta & -\Omega \delta & \Omega \delta & \Omega \delta & \Omega \sigma & \Omega \sigma & \Omega \sigma & -\mu + \Omega \sigma & \Omega \sigma \\ -\Lambda \delta & 0 & \Lambda \delta & 0 & \Lambda \sigma & \Lambda \sigma & \Lambda \sigma & \Lambda \sigma & -\mu + \Lambda \sigma \end{bmatrix} \quad (78)$$

with  $\sigma = (1 - \delta)$ ,  $\Xi = 2\lambda \frac{a_S^2 \varepsilon (1-f)}{a_S}$ ,  $\Pi = 2\lambda \frac{a_S^2 \varepsilon f}{a_S}$ ,  $\Delta = 2\lambda \frac{a_S^2 (1-f)}{a_S}$ ,  $\beta = 2\lambda \frac{a_S^2 f}{a_S}$ ,  $\phi = 4\lambda r \delta \frac{a_S \varepsilon}{a_S^2} H$ ,  $\Gamma = 4\lambda r \delta \frac{a_S f}{a_S^2} Y$ ,  $\Phi = 4\lambda r \delta \frac{a_S \varepsilon (1-f)}{a_S^2} Y$ ,  $H = \frac{(1-f)a_S^3}{1+2ra_S \delta \frac{a_S \varepsilon}{a_S}}$ ,  $Y = \frac{fa_S^3}{1+2ra_S \delta \frac{a_S \varepsilon (1-f) + a_S f}{a_S}}$ ,  $\Omega = \Delta - \phi$ ,  $\Sigma = \beta - \Phi$  and  $\Lambda = -\Gamma - \Phi + \beta$ .

The Jacobian matrix is a block matrix and we can consider separately the two blocks on the diagonal: the first block  $\mathbb{A}$  is triangular and the eigenvalues are  $\xi_{1,2} = -\mu_I$ ,  $\xi_{3,4,5,6,7,8} = -\mu$ ,  $\xi_{9,10} = -\gamma_P$ ,  $\xi_{11} = -\mu - \gamma_P$ ,  $\xi_{12,13} = -\mu - \gamma_A$  all negative. Therefore, it is sufficient to study block  $\mathbb{B}$ , which is a matrix  $9 \times 9$ . The epidemic threshold in the hybrid case is therefore obtained by numerically diagonalizing the matrix  $\mathbb{B}$  and imposing all its eigenvalues to be negative: this allows to obtain analytically the epidemic threshold for the hybrid CT for arbitrary  $\rho_S(a_S)$ ,  $\varepsilon(a_S)$  and  $f(a_S)$ .

## D. Limit cases

The obtained closed relations for the stability of the absorbing state in the manual and digital CT hold for arbitrary  $\rho_S(a_S)$ , for completely general  $f(a_S)$  and  $\varepsilon(a_S)$  and for general delays: this allows to introduce complicated effects, such as delay in isolation, activity heterogeneities and limited scalability of the system.

Due to the complicated structure of the equations for the stability (Eq. (25) and Eq. (63)), it is possible to derive the epidemic threshold  $r_C$  only by solving the equation numerically. However, there are some simple limit cases in which the equations are considerably simplified, allowing to obtain the epidemic threshold in an explicit analytic form.

### 1. Non-adaptive case (NA)

Here we consider the non-adaptive case, in which no adaptive behaviour are implemented, i.e. infected nodes behave as if they were susceptible, with  $(a_I, b_I) = (a_S, b_S)$ . Thus, in this case  $f(a_S) = \varepsilon(a_S) = 0$ ,  $\forall a_S$  and  $\gamma_P/\mu = 1$ . Replacing these values either in Eq. (25) or in Eq. (63) we obtain, as expected:

$$2ra_S^2 \overline{a_S} - \overline{a_S}^2 = 0$$

So we obtain an explicit form for the epidemic threshold  $r_C$  in the non-adaptive case:

$$r_C^{NA} = \frac{\overline{a_S}}{2a_S^2} \quad (79)$$

which is the Eq. (3) in the main paper. It reproduces the results previously obtained in Refs. [3, 5].

### 2. Isolation of only symptomatic nodes

Here we consider the case in which only symptomatic nodes are isolated as soon as they develops symptoms, i.e. no CT is implemented. Thus, in this case  $f(a_S) = \varepsilon(a_S) = 0$ ,  $\forall a_S$ , while  $(a_I, b_I) = (0, 0)$ . Replacing these values either in Eq. (25) or in Eq. (63) we obtain, as expected:

$$2ra_S^2 \overline{a_S} \left( \delta + (1 - \delta) \frac{\gamma_P}{\mu} \right) - \overline{a_S}^2 \frac{\gamma_P}{\mu} = 0$$

So we obtain an explicit form for the epidemic threshold  $r_C$ :

$$r_C^{SYMPTO} = r_C^{NA} \frac{\frac{\gamma_P}{\mu}}{\delta + (1 - \delta) \frac{\gamma_P}{\mu}} \quad (80)$$

which is the Eq. (4) in the main paper. For instantaneous symptoms development  $\gamma_P/\mu \rightarrow \infty$  it reproduces the results previously obtained in Ref. [5], and for  $\gamma_P/\mu = 1$  it reproduces the NA case (Eq. (79)).

### 3. Homogeneous case without delays and without limited scalability

Here we consider the case in which the population is homogeneous, i.e.  $\rho(a_S, b_S) = \delta(a_S - a)\delta(b_S - b)$ , with constant probability of downloading the app in digital CT, i.e.  $f(a_S) = f$ , and constant probability for a contact to be traced in manual CT, i.e.  $\varepsilon(a_S) = \varepsilon$ . Moreover we assume  $\tau_C = 0$ , that is  $\gamma_A = \gamma_P$ . Replacing these values in the Eq. (25), for the manual CT we obtain a quadratic equation in  $r$ :

$$4a^2\delta^2\varepsilon r^2 + 2a \left( \delta + \frac{\gamma_P}{\mu} (1 - \delta - \delta\varepsilon) \right) r - \frac{\gamma_P}{\mu} = 0$$

The equation can be solved and we obtain:

$$r_C^{MANUAL} = r_C^{NA} \frac{2\frac{\gamma_P}{\mu}}{\delta + (1 - \delta - \varepsilon\delta) \frac{\gamma_P}{\mu} + \sqrt{(\delta + (1 - \delta - \varepsilon\delta) \frac{\gamma_P}{\mu})^2 + 4\delta^2\varepsilon \frac{\gamma_P}{\mu}}} \quad (81)$$

which is the Eq. (5) in the main paper.

Analogously, replacing the values in the Eq. (63) for the digital CT we obtain an equation of second degree in  $r$ :

$$4a^2\delta f \left( \delta + \frac{\gamma_P}{\mu} (1 - \delta)(1 - f) \right) r^2 + 2a \left( \delta + \frac{\gamma_P}{\mu} (1 - \delta - \delta f) \right) r - \frac{\gamma_P}{\mu} = 0$$

The equation can be solved and we obtain:

$$r_C^{APP} = r_C^{NA} \frac{2\frac{\gamma_P}{\mu}}{\delta + (1 - \delta - f\delta) \frac{\gamma_P}{\mu} + \sqrt{(\delta + (1 - \delta - f\delta) \frac{\gamma_P}{\mu})^2 + 4\delta f \frac{\gamma_P}{\mu} (\delta + \frac{\gamma_P}{\mu} (1 - f)(1 - \delta))}} \quad (82)$$

which is the Eq. (6) in the main paper.

### 4. Heterogeneous case

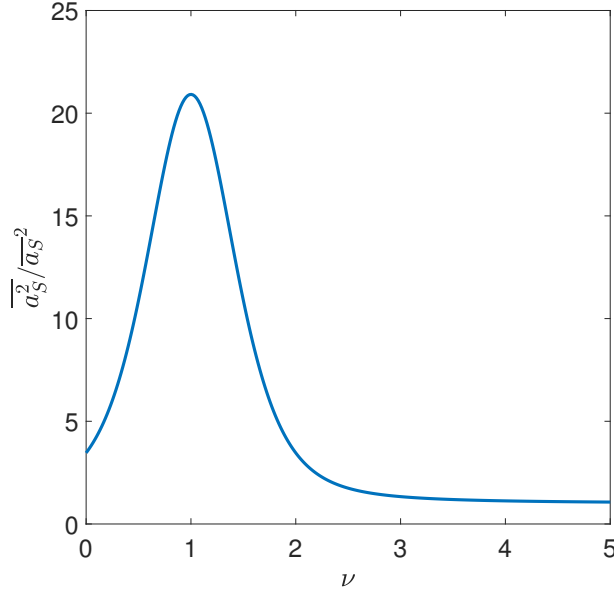
Hereafter and in the main text we consider a realistic heterogeneous population, i.e. a power-law activity distribution:

$$\rho(a_S, b_S) \sim a_S^{-(\nu+1)} \delta(b_S - a_S) \quad (83)$$

with  $a_S \in [a_m, a_M]$  and  $\eta = a_M/a_m$ , where  $a_m$  and  $a_M$  are respectively activity lower and upper cut-off.

Supplementary Fig. 2 shows that the considered distribution is maximally broad for  $\nu = 1$ : indeed, the ratio  $\frac{\overline{a_S^2}}{\overline{a_S}^2}$ , which we plot, provides a estimate of the heterogeneity and fluctuations of the distribution and it is maximized for  $\nu = 1$ . On the contrary for  $\nu \rightarrow 0$  the distribution is counterintuitively more homogeneous, due to cut-off effects and constraints imposed on the distribution ( $\overline{a_S}$  and  $\eta$  fixed), which thus set the maximum heterogeneous condition at  $\nu = 1$ .

In this heterogeneous case it is possible to derive the epidemic threshold  $r_C$  only numerically, due to the complex structure of the equations for the stability (Eq. (25) and Eq. (63)). Fig. 3(a,b) and Fig. 4(a,b) of the main text show that both manual and digital CT protocols are more effective when the population is heterogeneous, indeed the maximum gain in the epidemic threshold is for  $\nu \sim 1 - 1.5$ . However, the maximum does not occur exactly at  $\nu = 1$ , i.e. when the distribution is maximally broad. Indeed, the epidemic thresholds do not depend solely on activity fluctuations, i.e.  $\overline{a_S^2}$ , but also on higher order moments (as  $\overline{a_S^3}$ ), as shown by Eq. (25) and Eq. (63). Thus, the CT protocols are more effective in heterogeneous populations and the maximum gain in  $r_C$  also depends on higher order moments of  $\rho_S$  and on other model parameters, as shown in Supplementary Fig. 3(b-c).



Supplementary Fig. 2: **Heterogeneity of the activity distribution.** We plot the ratio  $\overline{a_S^2}/\overline{a_S}^2$  as a function of exponent  $\nu$ , considering  $\rho(a_S, b_S)$  given by Eq. (83) with  $a_S \in [a_m, a_M]$ ,  $\eta = a_M/a_m$  and fixing  $\eta = 10^3$ .

## II. Supplementary Method 2: Continuous time Gillespie-like algorithm for network dynamics and epidemic evolution

The network dynamics is performed by a continuous-time Gillespie-like algorithm [6]: we assign to each node the activity  $a_S$  and attractiveness  $b_S$  drawn from the joint distribution  $\rho(a_S, b_S)$ . Initially, the network evolves in the absorbing state, i.e. all nodes are susceptible and infection does not propagate, up to a relaxation time  $t_0$ , to reach the equilibrium of activation dynamics:

1. The first activation time,  $t_i$ , of each node  $i$  is drawn from  $\Psi_{a_S^i}(t_i) = a_S^i e^{-a_S^i t_i}$  at time  $t = 0$ .
2. The node  $i$  with the lowest  $t_i$  activates and connects  $m$  randomly-selected nodes, with probability proportional to their attractiveness  $b_S$ .
3. The next activation time  $t_i$  for node  $i$  is set to  $t_i + \tau$ , with  $\tau$  inter-event time drawn from  $\Psi_{a_S^i}(\tau)$ .
4. All links are destroyed and the process is iterated from point 2.

Then we start the epidemic and contact tracing dynamics as follows:

1. At time  $t = t_0$  the population is divided into a configuration of susceptible ( $S$ ) and infected ( $P$  or  $A$ ) nodes, moreover each node has an activation time  $t_i > t_0 = t$  obtained from the initial relaxation dynamics.
2. Node  $i$  with the lowest  $t_i$  activates. Asymptomatic ( $A$ ,  $T$  and  $Q$ ) and symptomatic nodes ( $I$ ) at time  $t$  recover at  $t_i$  with probability respectively  $1 - e^{-\mu(t_i-t)}$  and  $1 - e^{-\mu_I(t_i-t)}$ : recovered nodes change their activity and attractiveness into  $(a_R, b_R) = (a_S, b_S)$ . Traced nodes at time  $t$  are isolated at  $t_i$  with probability  $1 - e^{-(t_i-t)/\tau_C}$  (with  $\tau_C > 0$  for manual CT and  $\tau_C = 0$  for digital CT) and set their activity and attractiveness to zero  $(a_Q, b_Q) = (0, 0)$ .
3. Pre-symptomatic nodes at time  $t$  develop symptoms at  $t_i$  with probability  $1 - e^{-\gamma_P(t_i-t)}$ : they set to zero their activity and attractiveness  $(a_I, b_I) = (0, 0)$  and the contact tracing is activated.

**Manual CT:** the protocol is enabled for every symptomatic node. Every contact made in the last  $T_{CT}$  period has  $\varepsilon(a_S)$  probability of being identified and tested, with  $a_S$  activity of the symptomatic node. Every node tested and found infected asymptomatic  $A$  becomes traced  $T$ .

**Digital CT:** the protocol is enabled only if the symptomatic node has downloaded the app. Each contact made in the last  $T_{CT}$  period with an individual who downloaded the app is identified and tested. Every node tested and found infected asymptomatic  $A$  becomes traced  $T$ .

4. We set the actual time  $t = t_i$  and the active agent  $i$  generates exactly  $m$  links with  $m$  nodes randomly-chosen with probability proportional to their attractiveness  $b$  at time  $t$  (depending on their status and

isolation). The contacts are registered in the contact list of both nodes engaged in the connection. If the link involves a susceptible and an infected node ( $P$ ,  $A$  or  $T$ ), a contagion can occur with probability  $\lambda$  and the susceptible node becomes pre-symptomatic with probability  $\delta$  or asymptomatic with probability  $1 - \delta$ .

5. The new activation time of node  $i$  is  $t_i = t + \tau$  and it is obtained drawing the inter-event time  $\tau$  from the inter-event time distribution  $\Psi_{a^i}(\tau) = a^i e^{-a^i \tau}$ , where  $a^i$  is the activity of node  $i$  at time  $t$ . All the links are deleted and the process is iterated from point 2.

### III. Supplementary Notes: Robustness of the results

The advantage of the manual CT is robust relaxing many assumptions and changing most parameters in the modelling scheme.

#### A. Activity-attractiveness distribution, limited scalability parameters and delays

Supplementary Fig. 3(a) shows the distribution  $P(k)$  of the number of contacts made by an individual over a  $T_{CT}$  period and the distribution  $P(k_T)$  of the number of contacts  $k_T$  traced by an index case with manual CT in the presence of limited scalability (recall probability as Eq.(2) of the main paper with  $k_c = 130$  [7]), for a realistically heterogeneous population. The average number of contacts traced by an index case is approximately 10 – 60 (depending on  $\bar{\varepsilon} \sim 0.1 - 0.5$ ), consistent with the reported data [7, 8]. Analogous contact patterns are generated by changing  $k_C$  or other parameters of the activity distribution.

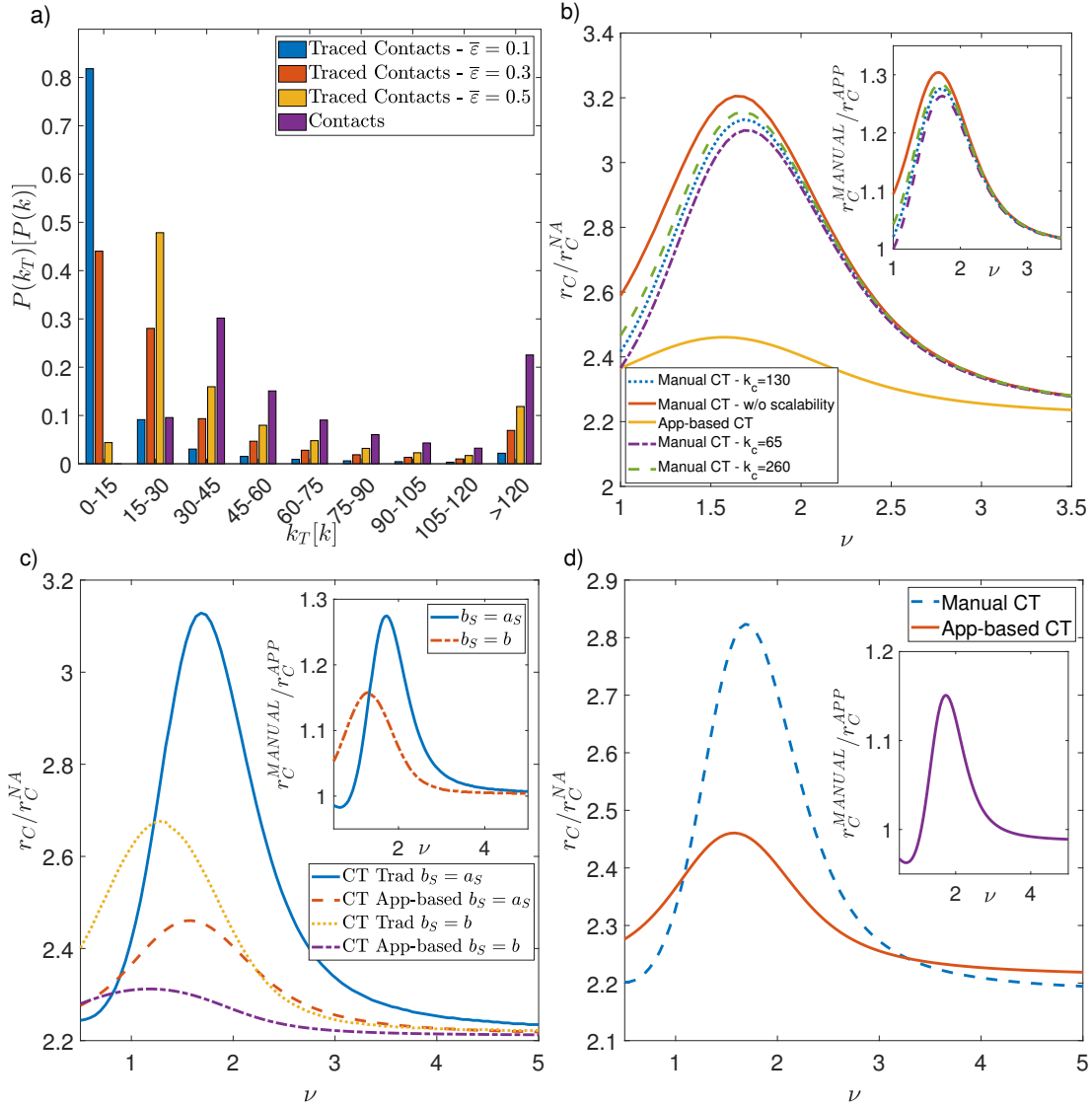
The results on the comparison between manual and digital CT are robust to changes in the maximum number of traceable contacts  $k_c$  in the manual CT: an increase in  $k_c$  reduces the effects of limited scalability; similarly, its reduction makes the effects of limited scalability stronger. However, modifying  $k_c$  with realistic values changes only slightly the epidemic threshold of the manual contact tracing protocol, without changing qualitatively the results, since the manual protocol remains more effective than the digital one, for small  $\bar{\varepsilon} = f^2$  values (Supplementary Fig. 3(b)).

The results are also robust when considering changes in the social properties of the population, i.e. assuming a different functional form of the  $\rho(a_S, b_S)$  distribution. For example, we can assume that all nodes feature equal attractiveness  $b$  and different activity:  $\rho(a_S, b_S) = \rho_S(a_S)\delta(b_S - b)$ . In this case the correlations between activity and attractiveness are removed: however, again the manual CT is more effective than the digital one in heterogeneous populations and for small  $\bar{\varepsilon} = f^2$  (Supplementary Fig. 3(c)). The differences between the two methods are reduced, compared to the case with correlations (see the inset of Supplementary Fig. 3(c)), due to the reduction in heterogeneities, since homogeneous terms are introduced assuming all the nodes having the same attractiveness. However, differences between the two protocols remain evident, even in the presence of delays  $\tau_C > 0$  and limited scalability in the manual CT.

Similarly, the advantage of manual contact tracing holds also considering limited scalability and stronger delays in manual contact tracing  $\tau_C$ : even for a delay of 7 days the manual CT remains more effective than the digital one, for small  $\bar{\varepsilon} = f^2$  and in heterogeneous populations (Supplementary Fig. 3(d)).

#### B. Epidemic active phase

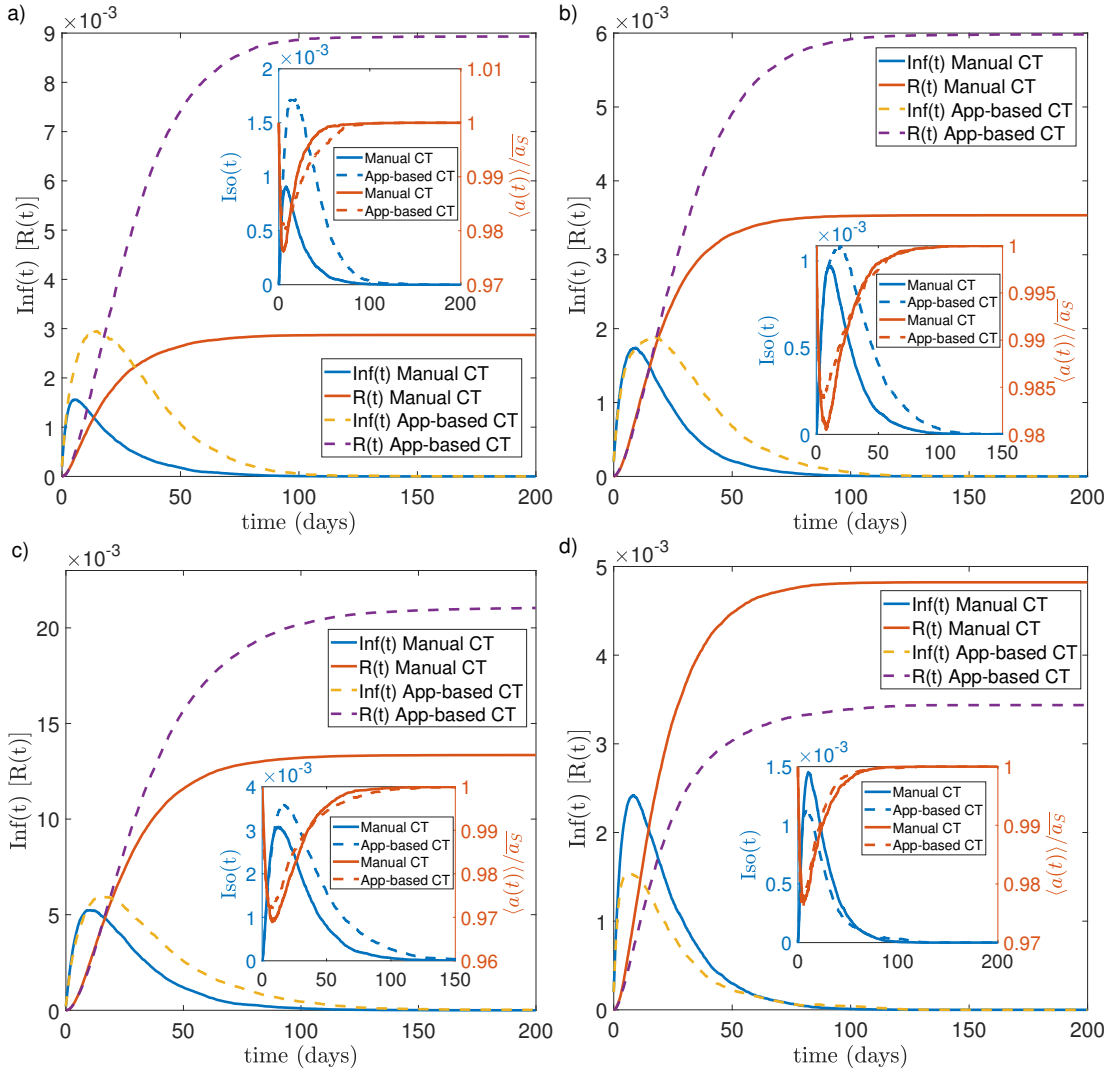
The results are also robust when considering the effects of contact tracing on the active phase of the epidemic: as expected from the analysis on the epidemic threshold, the differences between the two methods are reduced increasing  $\tau_C$ , however even with considerable delays  $\tau_C$  the manual CT for small values of  $\bar{\varepsilon} = f^2$  is more effective in flattening the infection peak and in lowering the epidemic final-size (Supplementary Fig. 4). Indeed, its effectiveness, compared to the digital CT, is maximized for  $\tau_C = 0$  (Supplementary Fig. 4(a)); the differences are reduced but still present considering strong delays in manual CT, such as  $\tau_C = 5$  days (Supplementary Fig. 4(b)). The differences remain even if we consider the system deeply in the active phase, that is for  $r \gg r_C$ : in this case the differences are slightly reduced due to the high infectivity of the system, however again the manual method for small  $\bar{\varepsilon}$  is more effective than digital CT (Supplementary Fig. 4(c)). Finally, as observed for the epidemic threshold, for very large  $\bar{\varepsilon} = f^2 = 0.6$  and strong delays  $\tau_C = 5$  days, the digital protocol becomes more effective in reducing the impact of the epidemic, further flattening the infection peak and reducing the epidemic final-size (Supplementary Fig. 4(d)). This again confirms that the effects of the protocols on the active phase are similar to those observed on the epidemic threshold, including the differences in the two approaches.



Supplementary Fig. 3: **Robustness of the results for the epidemic threshold.** In panel (a) we plot the distribution  $P(k)$  of contacts made by an individual over a  $T_{CT}$  period and the distribution  $P(k_T)$  of contacts traced by an index case with manual CT in the presence of limited scalability ( $k_C = 130$ ) for fixed  $\bar{\varepsilon}$  (see legend) and for  $\rho(a_S, b_S)$  given by Eq. (83) with  $\nu = 1$ . In panels (b)-(d) we plot the ratio between the epidemic threshold  $r_C$  in the presence of contact tracing protocols and the epidemic threshold of the non-adaptive case  $r_C^{NA}$ . The ratio is plotted for both manual and digital contact tracing, as a function of  $\nu$ . In all the insets we plot the ratio between the epidemic threshold of the manual contact tracing  $r_C^{MANUAL}$  and that of the app-based contact tracing  $r_C^{APP}$ , as a function of  $\nu$ . In panel (b) the ratio for the manual CT is plotted for several values of  $k_c$  and also when scalability is not considered (legend), setting  $\tau_C = 3$  days and  $\rho(a_S, b_S)$  given by Eq. (83). In panel (c) the ratio is plotted both for  $\rho(a_S, b_S) \sim a_S^{-(\nu+1)}\delta(b_S - a_S)$  and for  $\rho(a_S, b_S) \sim a_S^{-(\nu+1)}\delta(b_S - b)$  (legend), setting  $\tau_C = 3$  days and  $k_c = 130$ . In panel (d) the ratio is plotted for  $\rho(a_S, b_S)$  given by Eq. (83) setting  $\tau_C = 7$  days and  $k_c = 130$ . In all panels  $a_S \in [a_m, a_M]$  with  $a_M/a_m = 10^3$ ,  $\bar{a}_S = 6.7 \text{ days}^{-1}$ ,  $T_{CT} = 14$  days, and in panels (b)-(d)  $\bar{\varepsilon} = f^2 = 0.1$ ,  $\delta = 0.57$ ,  $\tau_P = 1.5$  days,  $\tau = 14$  days.

### C. Deterministic household CT

Typically when an individual becomes an index case, developing symptoms, her household is always traced and isolated, regardless of the CT protocol implemented. To take into account this effect, we augment both CT protocols with a deterministic contribution: a number of contacts, corresponding to the household, is always traced, both in digital and in manual CT. The augmented digital tracing is implemented by means of the hybrid CT formalism, assuming that the index case manually traces at least  $s$  contacts (household size) or, if she has had less, traces them all. The recall probability of this manual part is  $\varepsilon_h(a_S)$  defined as in Eq. (2) of the main paper, with  $k_C = s$  and  $\varepsilon_h^* = 1$ . The probability of tracing a contact within this augmented digital protocol is  $f^2 + \bar{\varepsilon}_h$  (where  $\bar{\varepsilon}_h = \int da_S \varepsilon_h(a_S) \rho_S(a_S)$ ): thus, to compare its efficacy with the manual CT, we fix the same probability to trace a contact, that is  $\bar{\varepsilon} = f^2 + \bar{\varepsilon}_h$ . In this way, even for the manual CT at least the tracing of



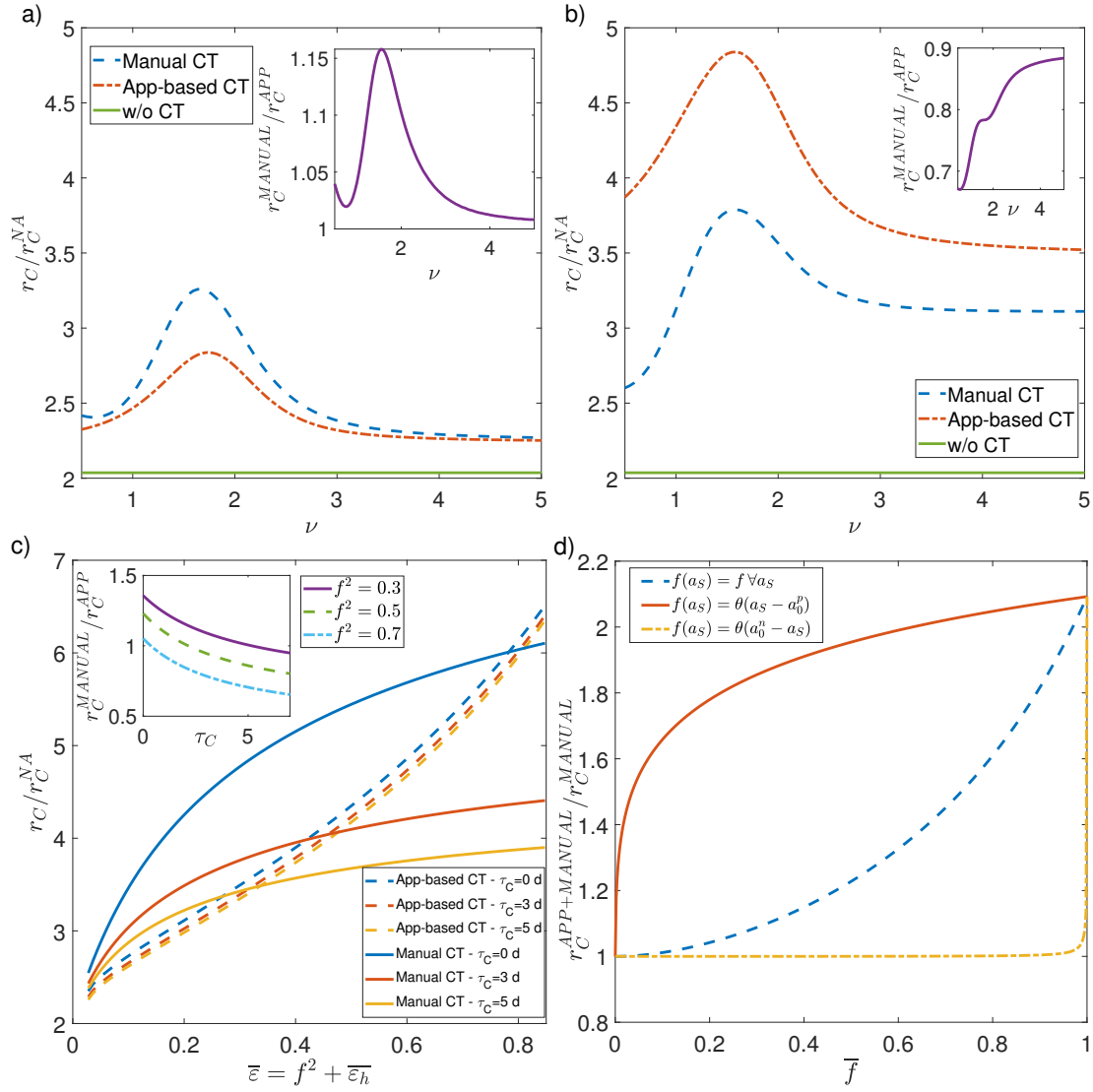
Supplementary Fig. 4: **Robustness of the results for the epidemic active phase.** In all panels we plot the temporal evolution of the fraction of infected nodes  $Inf(t)$ , i.e. infected asymptomatic and infected symptomatic, and of the fraction of removed nodes  $R(t)$ , for both manual and digital CT. In the insets we plot the temporal evolution of the fraction of isolated nodes  $Iso(t)$  (right y-axis) and of the average activity of the population  $\langle a(t) \rangle / \langle a_S \rangle$  (left y-axis), normalized with  $\bar{a}_S$ . All curves are averaged on several realization of disorder and temporal evolution. In panel (a) we set  $\tau_C = 0$ ,  $\bar{\varepsilon} = f^2 = 0.1$ ,  $r/r_C^{NA} = 4.0$  and the curves for digital and manual CT are averaged respectively over 379 and 445 realizations; in panel (b) we set  $\tau_C = 5$  days,  $\bar{\varepsilon} = f^2 = 0.1$ ,  $r/r_C^{NA} = 3.1$  and the curves for digital and manual CT are averaged respectively over 554 and 604 realizations; in panel (c) we set  $\tau_C = 5$  days,  $\bar{\varepsilon} = f^2 = 0.1$ ,  $r/r_C^{NA} = 7.0$  and the curves for digital and manual CT are averaged respectively over 311 and 348 realizations; in panel (d) we set  $\tau_C = 5$  days,  $\bar{\varepsilon} = f^2 = 0.6$ ,  $r/r_C^{NA} = 4.5$  and the curves for digital and manual CT are averaged respectively over 552 and 469 realizations. In all panels  $\rho(a_S, b_S)$  is given by Eq. (83) with  $a_S \in [a_m, a_M]$ ,  $a_M/a_m = 10^3$ ,  $\nu = 1.5$ ,  $\bar{a}_S = 6.7 \text{ days}^{-1}$ ,  $N = 5 \cdot 10^3$ ,  $\delta = 0.57$ ,  $\tau_P = 1.5$  days,  $\tau = 14$  days,  $k_c = 130$ ,  $T_{CT} = 14$  days and the errors, evaluated through the standard deviation, are smaller or comparable with the curves thickness.

the household is necessarily performed.

Supplementary Fig. 5(a)-(c) shows that for low values of  $\bar{\varepsilon} = f^2 + \bar{\varepsilon}_h$  (i.e. small  $f^2$ ) manual CT is more advantageous than the digital one, even taking into account the deterministic tracing of contacts in the household. The digital protocol becomes more effective only for high app adoption rates and unrealistic long delays: therefore, our results are robust to the addition of this deterministic household CT contribution.

#### D. Correlation between probability of app adoption and individual activity

We considered the probability of downloading the app uniform over the population, since economic and personal factors can produce opposite forces which correlate and anticorrelate the probability of downloading the app with the individuals' activity. Moreover personal data of CT app users are not available, due to privacy



Supplementary Fig. 5: **Effects of deterministic household contact tracing and effects of correlations between app adoption and activity.** In panels (a) and (b) we plot, as a function of the exponent  $\nu$ , the ratio between the epidemic threshold  $r_C$  for both CT protocols and the epidemic threshold of the non-adaptive case  $r_C^{NA}$ , with limited scalability, delay in manual CT and the additional deterministic household CT. In the insets we plot the ratio between the epidemic threshold of the augmented manual CT,  $r_C^{MANUAL}$ , and that of the augmented app-based CT,  $r_C^{APP}$ , as a function of  $\nu$ . In panel (a)  $f^2 = 0.1$  and  $\tau_C = 3$  days, while in panel (b)  $f^2 = 0.6$  and  $\tau_C = 5$  days. In panel (c) we plot the ratio  $r_C/r_C^{NA}$  as a function of  $\bar{\varepsilon} = f^2 + \bar{\varepsilon}_h$  for both augmented CT protocols, setting  $\nu = 1.5$  and for several values of  $\tau_C$ : in the inset we plot the ratio  $r_C^{MANUAL}/r_C^{APP}$  as a function of  $\tau_C$  for several  $f^2$  values. In all panels (a)-(c) we fix  $s = 3$  (size of household) and  $\varepsilon_h^* = 1$ , corresponding to  $\bar{\varepsilon}_h = 0.028$ . In panel (d) we plot, as a function of  $\bar{f}$ , the ratio between  $r_C^{MANUAL+APP}$ , the epidemic threshold when the hybrid CT protocol is implemented, and  $r_C^{MANUAL}$ , the epidemic threshold when only the manual CT is implemented. The curves correspond to the uncorrelated, positively correlated and negatively correlated  $f(a_S)$  (see legend), and are obtained fixing  $\bar{\varepsilon} = 0.4$ ,  $\tau_C = 3$  days,  $\nu = 1.5$ . In all panels the distribution  $\rho(a_S, b_S)$  is given by Eq. (83),  $a_M/a_m = 10^3$ ,  $\bar{a}_S = 6.7 \text{ days}^{-1}$ ,  $\delta = 0.57$ ,  $\tau_P = 1.5$  days,  $\tau = 14$  days,  $k_c = 130$ ,  $T_{CT} = 14$  days.

issues. However, evidences are currently emerging that those who download the app are individuals who engage very cautious behaviors, i.e.  $f$  and  $a_S$  are anticorrelated [9, 10].

We implement the hybrid CT protocol on a heterogeneous population, investigating the effectiveness of digital CT varying the app adoption level  $\bar{f} = \int da_S f(a_S) \rho_S(a_S)$  and the correlations between  $f$  and  $a_S$ . We consider three extreme cases of correlations: the uncorrelated case in which  $f(a_S) = \bar{f} = f \forall a_S$ ; the completely positively correlated case  $f(a_S) = \theta(a_S - a_0^p)$ , with  $\theta(x)$  the Heaviside step function; the completely negatively correlated case  $f(a_S) = \theta(a_0^n - a_S)$ . These borderline cases are hardly realistic, however they allow to obtain useful information on the role of correlations: more realistic shapes of  $f(a_S)$  are interesting directions for future work.

To compare these three cases, we set the thresholds  $a_0^n$  and  $a_0^p$  by fixing  $\bar{f}$ : Supplementary Fig. 5(d) shows that correlations have a strong impact on the effectiveness of digital CT. If the app is downloaded from all hubs

(positive correlations) a low level of adoption  $\bar{f} \sim 0$  is enough to obtain a significant increase in the epidemic threshold; on the contrary, if the app is downloaded only by very cautious people (negative correlations) the effect of the digital CT becomes significant only for very high adoption level  $\bar{f} \sim 1$ , worse than the uncorrelated case.

The effects of correlations in app adoption further strengthens our results, highlighting the dominant role of manual CT in the current situation of negative correlations [9, 10]. Furthermore these results suggest future directions to make digital CT more effective exploiting heterogeneities.

## Supplementary References

- [1] Mancastropa, M., Vezzani, A., Muñoz, M. A. & Burioni, R. Burstiness in activity-driven networks and the epidemic threshold. *J. Stat. Mech.: Theory Exp* **2019**, 053502 (2019).
- [2] Tizzani, M. *et al.* Epidemic spreading and aging in temporal networks with memory. *Phys. Rev. E* **98**, 062315 (2018).
- [3] Pozzana, I., Sun, K. & Perra, N. Epidemic spreading on activity-driven networks with attractiveness. *Phys. Rev. E* **96**, 042310 (2017).
- [4] Ghoshal, G. & Holme, P. Attractiveness and activity in internet communities. *Physica A* **364**, 603 – 609 (2006).
- [5] Mancastropa, M., Burioni, R., Colizza, V. & Vezzani, A. Active and inactive quarantine in epidemic spreading on adaptive activity-driven networks. *Phys. Rev. E* **102**, 020301 (2020).
- [6] Gillespie, D. T. A general method for numerically simulating the stochastic time evolution of coupled chemical reactions. *J. Comput. Phys.* **22**, 403 – 434 (1976).
- [7] Keeling, M. J., Hollingsworth, T. D. & Read, J. M. Efficacy of contact tracing for the containment of the 2019 novel coronavirus (covid-19). *J. Epidemiology Community Health* **74**, 861–866 (2020).
- [8] Visontay, E. Victoria’s contact-tracing effort buckles under the weight of covid-19 cases. *The Guardian* (2020). 08-04-2020.
- [9] von Wyl, V. *et al.* Drivers of acceptance of covid-19 proximity tracing apps in Switzerland: panel survey analysis. *JMIR Public Health Surveill.* **7**, e25701 (2021).
- [10] Saw, Y. E., Tan, E. Y., Liu, J. S. & Liu, J. C. Predicting public uptake of digital contact tracing during the covid-19 pandemic: results from a nationwide survey in Singapore. *J. Med. Internet Res.* **23**, e24730 (2021).